

1 **A non-equilibrium model for soil heating and moisture transport during**
2 **extreme surface heating**

3 W. J. Massman
4 USDA Forest Service
5 Rocky Mountain Research Station
6 240 West Prospect
7 Fort Collins, CO 80526 USA
8 email: wmassman@fs.fed.us

9 September 2015

10 **Abstract.** Increased use of prescribed fire by land managers and the increasing likelihood
11 of wildfires due to climate change require an improved modeling capability of extreme heat-
12 ing of soils during fires. This issue is addressed here by developing and testing a 1-D non-
13 equilibrium (liquid-vapor phase change) model of soil evaporation that simulates the coupled
14 simultaneous transport of heat, soil moisture, and water vapor. This model is intended for
15 use with surface forcing ranging from daily solar cycles to extreme conditions encountered
16 during fires. It employs a linearized Crank-Nicolson scheme for the conservation equations
17 of energy and mass and its performance is evaluated against dynamic soil temperature and
18 moisture observations, which were obtained during laboratory experiments on soil samples
19 exposed to surface heat fluxes ranging between 10,000 and 50,000 Wm^{-2} . The Hertz-Knudsen
20 equation is the basis for constructing the model's non-equilibrium evaporative source term.
21 Some unusual aspects of the model that were found to be extremely important to the model's
22 performance include: (1) a dynamic (temperature and moisture potential dependent) con-
23 densation coefficient associated with the evaporative source term, (2) an infrared radiation
24 component to the soil's thermal conductivity, and (3) a dynamic residual soil moisture. This
25 last term, which is parameterized as a function of temperature and soil water potential, is
26 incorporated into the water retention curve and hydraulic conductivity functions in order
27 to improve the model's ability to capture the evaporative dynamics of the strongly bound
28 soil moisture, which requires temperatures well beyond 150 C to fully evaporate. The model
29 also includes film flow, although this phenomenon did not contribute much to the model's
30 overall performance. In general, the model simulates the laboratory-observed temperature
31 dynamics quite well, but is less precise (but still good) at capturing the moisture dynamics.
32 The model emulates the observed increase in soil moisture ahead of the drying front and
33 the hiatus in the soil temperature rise during the strongly evaporative stage of drying. It
34 also captures the observed rapid evaporation of soil moisture that occurs at relatively low

35 temperatures (50-90 C), and can provide quite accurate predictions of the total amount of
36 soil moisture evaporated during the laboratory experiments. The model's solution for water
37 vapor density (and vapor pressure), which can exceed one standard atmosphere, cannot be
38 experimentally verified, but they are supported by results from (earlier and very different)
39 models developed for somewhat different purposes and for different porous media. Over-
40 all, this non-equilibrium model provides a much more physically realistic simulation over a
41 previous equilibrium model developed for the same purpose. Current model performance
42 strongly suggests that it is now ready for testing under field conditions.

43 1. Introduction

44 Since the development of the theory of Philip and de Vries (PdV model) almost 60
45 years ago [*Philip and de Vries* 1957; *de Vries* 1958] virtually all models of evaporation and
46 condensation in unsaturated soils have assumed that soil water vapor at any particular depth
47 into the soil is in equilibrium with the liquid soil water (or soil moisture) at the same depth.
48 (Note: such soil evaporation models also assume thermal equilibrium, so that at any given
49 depth the mineral soil, the soil moisture, and the soil air and water vapor within the pore
50 space are also at the same temperature.) In essence, this local equilibrium assumption means
51 that whenever the soil moisture changes phase it does so instantaneously. This assumption
52 is quite apropos for its original application, which was to describe the coupled heat and
53 moisture transport in soils (and soil evaporation in particular) under environmental forcings
54 associated with the daily and seasonal variations in radiation, temperature, precipitation,
55 etc. [e.g., *Milly* 1982; *Novak* 2010; *Smits et al.* 2011]. Under these conditions assuming
56 local equilibrium is reasonable because the time required to achieve equilibrium after a
57 change of phase is ‘instantaneous’ (short) relative to the time scale associated with normal
58 environmental forcing. The great benefit to the equilibrium assumption is that for modeling
59 purposes it is a significant simplification to the equations that describe heat and moisture
60 flow in soils because it eliminates the need to include soil water vapor density, ρ_v , as an
61 independent model variable. More formally, under equilibrium ρ_v is directly equated to the
62 equilibrium vapor density, a function only of local soil temperature and soil water content
63 (or more specifically the soil water potential).

64 Subsequent to the development of the original PdV model the equilibrium assumption
65 has also been incorporated into models of heat and moisture transport (evaporation and
66 condensation) in soils and other porous media under more extreme forcings associated with
67 high temperatures and heat fluxes. For example, it has been applied to (*i*) soils during

68 wildfires and prescribed burns [*Aston and Gill* 1976; *Campbell et al.* 1995; *Durany et al.*
69 2010; *Massman* 2012], (ii) drying of wood [*Whitaker* 1977; *di Blasi* 1997], (iii) drying and
70 fracturing of concrete under high temperatures [*Dayan* 1982; *Dal Pont et al.* 2011], (iv)
71 high temperature sand-water-steam systems [e.g., *Udell* 1983; *Bridge et al.* 2003], and (v)
72 evaporation of wet porous thermal barriers under high heat fluxes [*Costa et al.* 2008].

73 Although the PdV model and the equilibrium assumption have certainly led to many
74 insights into moisture and vapor transport and evaporation in porous media, it has, nonethe-
75 less, yielded somewhat disappointing simulations of the coupled soil moisture dynamics dur-
76 ing fires [see *Massman* 2012 for further details and general modeling review]. Possibly
77 the most interesting of these modeling “disappointments” is the soil/fire-heating model of
78 *Massman* [2012], who found that as the soil moisture evaporated it just re-condensed and
79 accumulated ahead of the dry zone; consequently, no water actually escaped the soil at all,
80 which, to say the least, seems physically implausible! He further traced the cause of this
81 anomalous behavior to the inapplicability of the equilibrium evaporation assumption, which
82 allowed the soil vapor gradient behind the drying front to become so small that the soil
83 vapor could not escape (diffuse) out of the soil. Or, more fundamentally, the calculated
84 vapor and its attendant gradient became largely meaningless because it is impossible for
85 water vapor to be in equilibrium with liquid water if there is no liquid water. Of course,
86 such extremely dry conditions are just about guaranteed during soil heating events like fires.
87 *Novak* [2012] also recognized the inapplicability of the equilibrium assumption for very dry
88 soils, but under more normal environmental forcing. On the other hand, even under normal
89 (and much less extreme) soil moisture conditions both *Smits et al.* [2011] and *Ouedraogo*
90 *et al.* [2013] suggest that non-equilibrium formulations of soil evaporation may actually im-
91 prove model performance, which implies that the non-equilibrium assumption may really be
92 a more appropriate description for soil evaporation and condensation than the equilibrium

93 assumption. The present study is intended to provide the first test of the non-equilibrium
94 hypothesis during extreme conditions.

95 Specifically, the present study develops and evaluates a non-equilibrium (liquid-vapor
96 phase change) model for simulating coupled heat, moisture, and water vapor transport during
97 extreme heating events. It also assumes thermal equilibrium between the soil solids, liquid,
98 and vapor. It uses a systems-theoretic approach [e.g., *Gupta and Nearing 2014*] focused more
99 on physical processes than simply tuning model parameters, which here means that whatever
100 model or parameter “tuning” does occur it is intended to keep the model numerically stable
101 and as physically realistic as possible.

102 In addition, the present study (model) is a companion to *Massman [2012]*. It uses much
103 of the same notation as the earlier study. But, unlike its predecessor, this study allows for
104 the possibility of liquid water movement (i.e., it includes a hydraulic conductivity function
105 for capillary and film flow). It also improves on and corrects (where possible and as noted in
106 the text) the mathematical expressions used in the previous paper to parameterize the high
107 temperature dependency of latent heat of vaporization, saturation vapor density, diffusivity
108 of water vapor, soil thermal conductivity, water retention curve, etc. This is done in order to
109 achieve the best representation of the physical properties of water (liquid and vapor) under
110 high temperatures and pressures [see, e.g., *Harvey and Friend 2004*]. And lastly, in order to
111 facilitate comparing the present model with the earlier companion model the present study
112 displays all graphical results in a manner very similar to those of *Massman [2012]*.

113 **2. Model Development**

114 The present model is one-dimensional (in the vertical) and is developed from three coupled
115 partial differential equations. It allows for the possibility that the soil liquid and vapor
116 concentrations are not necessarily in local equilibrium during evaporation/condensation, but
117 it does assume local thermal equilibrium during any phase change. The present model has

118 three simulation variables: soil temperature ($\equiv T$ [C] or T_K [K]); soil water potential ($\equiv \psi$ [J
 119 kg^{-1}] or $\psi_n \equiv$ normalized soil water potential [*dimensionless*]; and vapor density ($\equiv \rho_v$ [kg
 120 m^{-3}]). Here $\psi_n = \psi/\psi_*$ and $\psi_* = -10^6$ [J kg^{-1}], which *Campbell et al.* [1995] identify as the
 121 water potential for oven dry soil. This current model employs a linearized Crank-Nicolson [C-
 122 N] finite difference scheme, whereas the preceding (companion) model [*Massman* 2012] used
 123 the Newton-Raphson method for solving the fully implicit finite difference equations. The
 124 present model further improves on its companion by including the possibility of soil water
 125 movement (hydraulic conductivity function driven by a gradient in soil moisture potential)
 126 and better parameterizations of thermophysical properties of water and water vapor. These
 127 latter parameterizations allow for the possibility of large variations in the amount of soil water
 128 vapor, which *Massman* [2012] suggests might approach or exceed one standard atmosphere
 129 and therefore could become the major component of the soil atmosphere during a heating
 130 event. This is quite unlike any other model of soil heat and moisture flow, which universally
 131 assume that dry air is the dominant component of the soil atmosphere and that water vapor
 132 is a relatively minor component. Finally, and also atypical of most other soil models, the
 133 model's water retention curve and hydraulic function include a dynamic residual soil moisture
 134 content as a function of soil temperature and soil water potential.

135 2.1 Conservation Equations

136 The conservation of thermal energy is expressed as:

$$C_s \frac{\partial T}{\partial t} - \frac{\partial}{\partial z} \left[\lambda_s \frac{\partial T}{\partial z} \right] + (\eta - \theta) \rho_a c_{pa} u_{vl} \frac{\partial T}{\partial z} = -L_v S_v \quad (1)$$

137

138 where t [s] is time; z [m] is soil depth (positive downward); T is soil temperature in Celsius;
 139 $C_s = C_s(\theta, T)$ [J m^{-3} K^{-1}] is the volumetric heat capacity of soil, a function of both soil
 140 temperature and soil volumetric water content θ [$\text{m}^3 \text{m}^{-3}$]; $\lambda_s = \lambda_s(\theta, T, \rho_v)$ [W m^{-1} K^{-1}]

141 is the thermal conductivity of the soil, a function of soil temperature, soil moisture, and
 142 soil vapor density; η [m^3m^{-3}] is the total soil porosity from which it follows that $(\eta - \theta)$ is
 143 the soil's air filled porosity; $\rho_a = \rho_a(T_K, \rho_v)$ [kg m^{-3}] is the mass density of the soil air, a
 144 function of temperature and soil vapor density; $c_{pa} = c_{pa}(T_K, \rho_v)$ [$\text{J kg}^{-1} \text{K}^{-1}$] is specific heat
 145 capacity of ambient air, also a function of temperature and vapor density; u_{vl} [m s^{-1}] is the
 146 advective velocity induced by the change in volume associated with the rapid volitalization
 147 of soil moisture (detailed below); $L_v = L_v(T_K, \psi)$ [J kg^{-1}] is the latent heat of vaporization;
 148 and $S_v = S_v(T_K, \theta, \psi, \rho_v)$ [$\text{kg m}^{-3} \text{s}^{-1}$] is the source term for water vapor.

149 The conservation of mass for liquid water is

$$\frac{\partial(\rho_w\theta)}{\partial t} - \frac{\partial}{\partial z} \left[\rho_w K_n \frac{\partial\psi_n}{\partial z} + \rho_w K_H - \rho_w V_{\theta,surf} \right] = -S_v \quad (2)$$

150

151 $\rho_w = \rho_w(T_K)$ [kg m^{-3}] is the density of liquid water; $K_n = K_n(T_K, \psi, \theta)$ [$\text{m}^2 \text{s}^{-1}$] is the
 152 hydraulic diffusivity; $K_H = K_H(T_K, \psi, \theta)$ [m s^{-1}] is the hydraulic conductivity; and $V_{\theta,surf} =$
 153 $V_{\theta,surf}(T_K, \theta)$ [m s^{-1}] is the velocity of liquid water associated with surface diffusion of water,
 154 which may be significant at high temperatures [e.g., *Kapoor et al.* 1989; *Medveď and Černý*
 155 2011]. Note that switching variables from $\psi < 0$, to ψ_n produces $\psi_n > 0$ and $K_n < 0$.

156 This last equation can be simplified to

$$\rho_w \frac{\partial\theta}{\partial t} - \rho_w \frac{\partial}{\partial z} \left[K_n \frac{\partial\psi_n}{\partial z} + K_H - V_{\theta,surf} \right] = -S_v \quad (3)$$

157

158 because $\frac{1}{\rho_w} \frac{d\rho_w}{dT}$ varies by only 4% between about 10 C to 100 C the derivatives $\frac{\partial\rho_w}{\partial t} \equiv \frac{d\rho_w}{dT} \frac{\partial T}{\partial t}$
 159 and $\frac{\partial\rho_w}{\partial z} \equiv \frac{d\rho_w}{dT} \frac{\partial T}{\partial z}$ can be ignored. But the model does retain the temperature dependency
 160 $\rho_w = \rho_w(T_K)$, except as noted in the section below on volumetric specific heat capacity of
 161 soil, and it also specifically includes $d\rho_w/dT$ for other components of the model.

162 The conservation of mass for water vapor is

$$\frac{\partial(\eta - \theta)\rho_v}{\partial t} - \frac{\partial}{\partial z} \left[D_{ve} \frac{\partial \rho_v}{\partial z} - (\eta - \theta)u_{vl}\rho_v \right] = S_v \quad (4)$$

163

164 where $D_{ve} = D_{ve}(T_K, \psi, \rho_v)$ [$\text{m}^2 \text{s}^{-1}$] is the (equivalent) molecular diffusivity associated with
 165 the diffusive transport of water vapor in the soil's air-filled pore space. As with *Massman*
 166 [2012], the present model also expresses Fick's first law of diffusion in terms of mass, i.e.,
 167 the diffusive flux $J_{diff} = J_{diff}^{[Mass]} = -D_{ve}\partial\rho_v/\partial z$. But there are other forms that could
 168 have been used. For example, *Campbell et al.* [1995] use a form discussed by *Cowan* [1977]
 169 and *Jones* [2014], i.e., $J_{diff} = J_{diff}^{[Pressure]} = -D_{ve}[M_w/(RT_K)]\partial e_v/\partial z$; where e_v [Pa] is the
 170 vapor pressure, $M_w = 0.01802 \text{ kg mol}^{-1}$ is the molar mass of water vapor, and $R = 8.314$
 171 $\text{Jmol}^{-1}\text{K}^{-1}$ is the universal gas constant. Yet again, *Jaynes and Rogowski* [1983] suggest that
 172 $J_{diff} = J_{diff}^{[Fraction]} = -D_{ve}(\rho_v + \rho_d)\partial\omega_v/\partial z$ may be the more appropriate expression for J_{diff} ;
 173 where ρ_d [kg m^{-3}] is the dry air density (defined and discussed later) and $\omega_v = \rho_v/(\rho_v + \rho_d)$
 174 [kg kg^{-1}] is the mass fraction of water vapor within the soil pore space. The distinctions
 175 between these different formulations of Fick's first law is important to the present work
 176 because different forms of J_{diff} can yield different numerical values for the fluxes [e.g., *Solsvik*
 177 *and Jakobsen* 2012] that can diverge significantly with large temperature gradients. This
 178 issue is examined in more detail in a later section devoted to the model's sensitivity to
 179 different modeling assumptions and performance relative to different data sets and input
 180 parameters.

181 The final model equations are expressed in terms of the model variables (T, ψ_n, ρ_v) and
 182 result from: (a) expanding the spatial derivative $\frac{\partial K_H}{\partial z}$ in terms of the spatial derivatives $\frac{\partial T}{\partial z}$
 183 and $\frac{\partial \psi_n}{\partial z}$, (b) allowing for $\theta = \theta(\psi_n, T_K)$, (c) combining Equation (3) with (1) and Equation
 184 (4) with (3), and (d) simplifying Equation (4). These equations are

$$(C_s - L_v \rho_w D_{\theta T}) \frac{\partial T}{\partial t} - \frac{\partial}{\partial z} \left[\lambda_s \frac{\partial T}{\partial z} \right] + \left[(\eta - \theta) \rho_a c_{pa} u_{vl} + L_v \rho_w \frac{\delta K_H}{\delta T_K} \right] \frac{\partial T}{\partial z} + L_v \rho_w \frac{\partial}{\partial z} \left[K_m \frac{\partial T}{\partial z} \right]$$

185

$$- L_v \rho_w D_{\theta \psi} \frac{\partial \psi_n}{\partial t} + L_v \rho_w \frac{\partial}{\partial z} \left[K_n^* \frac{\partial \psi_n}{\partial z} \right] + L_v \rho_w \left[\frac{\partial K_H}{\partial \psi_n} \right] \frac{\partial \psi_n}{\partial z} = 0 \quad (5)$$

186

187 which is the conservation of energy;

$$\begin{aligned} & \rho_w D_{\theta T} \frac{\partial T}{\partial t} - \rho_w \frac{\partial}{\partial z} \left[K_m \frac{\partial T}{\partial z} \right] - \rho_w \left[\frac{\delta K_H}{\delta T_K} \right] \frac{\partial T}{\partial z} \\ & + \rho_w D_{\theta \psi} \frac{\partial \psi_n}{\partial t} - \rho_w \frac{\partial}{\partial z} \left[K_n^* \frac{\partial \psi_n}{\partial z} \right] - \rho_w \left[D_{\theta \psi} \frac{\partial K_H}{\partial \theta} \right] \frac{\partial \psi_n}{\partial z} \end{aligned}$$

188

$$+ (\eta - \theta) \frac{\partial \rho_v}{\partial t} - \frac{\partial}{\partial z} \left[\mathcal{D}_v \frac{\partial \rho_v}{\partial z} - (\eta - \theta) u_{vl} \rho_v \right] = 0 \quad (6)$$

189

190 which is the conservation of soil moisture; and

$$- \rho_v D_{\theta T} \frac{\partial T}{\partial t} + (\eta - \theta) \frac{\partial \rho_v}{\partial t} - \frac{\partial}{\partial z} \left[\mathcal{D}_v \frac{\partial \rho_v}{\partial z} - (\eta - \theta) u_{vl} \rho_v \right] - \rho_v D_{\theta \psi} \frac{\partial \psi_n}{\partial t} = S_v \quad (7)$$

191

192 which is the conservation of mass for water vapor.

193 Apropos to these last three equations: (i) $D_{\theta \psi} = \partial \theta / \partial \psi_n$ and $D_{\theta T} = \partial \theta / \partial T_K$ are obtained
 194 from the water retention curve (WRC); (ii) $\frac{\delta K_H}{\delta T_K} = \left[\frac{\partial K_H}{\partial T_K} + \frac{\partial K_H}{\partial \theta} D_{\theta T} \right]$; (iii) K_m [$\text{m}^2 \text{s}^{-1} \text{K}^{-1}$]
 195 and K_n^* [$\text{m}^2 \text{s}^{-1}$] (which subsumes K_n) are related to $V_{\theta, surf}$ and are defined in a later section;
 196 (iv) because $\rho_v \ll \rho_w$ the term $(\rho_w - \rho_v) \frac{\partial \theta}{\partial t}$ originally in Equation (6) has been approximated

197 by $\rho_w \frac{\partial \theta}{\partial t} \equiv \rho_w D_{\theta\psi} \frac{\partial \psi_n}{\partial t} + \rho_w D_{\theta T} \frac{\partial T}{\partial t}$; and (v) the total porosity η is assumed to be spatially
 198 uniform and temporally invariant.

199 2.2 Functional Parameterizations

200 2.2.1 Thermophysical Properties of Water, Vapor, and Moist Air

201 The algorithm for calculating water density, $\rho_w(T_K)$, is Equation (2.6) of *Wagner and*
 202 *Pruess* [2002] and employed only within the temperature range $273.15 \text{ K} \leq T_K \leq 383.15$
 203 K ($\equiv T_{K,max}$). At temperatures greater than $T_{K,max}$, then $\rho_w(T_K) = \rho_w(T_{K,max})$. This
 204 approach yields a range for $\rho_w(T_K)$ of $950 \text{ kg m}^{-3} < \rho_w(T_K) < 1000 \text{ kg m}^{-3}$, which represents
 205 a compromise between the fact that the density of (free saturated liquid) water continues to
 206 decrease with increasing temperatures [*Yaws* 1995] and the hypothetical possibility that in
 207 a bound state a mono-layer of liquid water $\rho_w(T_K)$ may reach values as high as $\approx 5000 \text{ kg}$
 208 m^{-3} [*Danielewicz-Ferchmin and Mickiewicz* 1996]. $d\rho_w/dT$ is computed from the analytical
 209 expression derived by differentiating the expression for $\rho_w(T_K)$ and $d\rho_w/dT = 0$ for $T_K >$
 210 $T_{K,max}$.

211 The enthalpy of vaporization of water, $H_v = H_v(T_K, \psi)$ [J mol^{-1}], is Equation (5) of
 212 *Somayajulu* [1988] augmented by the soil moisture potential, ψ , [*Massman* 2012; *Campbell*
 213 *et al.* 1995] and is expressed as follows:

$$H_v = H_1 \left(\frac{T_{crit} - T_K}{T_K} \right) + H_2 \left(\frac{T_{crit} - T_K}{T_{crit}} \right)^{\frac{3}{8}} + H_3 \left(\frac{T_{crit} - T_K}{T_{crit}} \right)^{\frac{9}{4}} - M_w \psi \quad (8)$$

214

215 where $H_1 = 13.405538 \text{ kJ mol}^{-1}$, $H_2 = 54.188028 \text{ kJ mol}^{-1}$, $H_3 = -58.822461 \text{ kJ mol}^{-1}$,
 216 and $T_{crit} = 647.096 \text{ K}$ is the critical temperature for water. Note that $h_v = h_v(T_K)$ [J
 217 mol^{-1}] will denote the enthalpy of vaporization without the additional $-M_w \psi$ term, i.e.,
 218 $h_v = h_v(T_K) = H_1 (T_{crit} - T_K) / T_K + H_2 [(T_{crit} - T_K) / T_{crit}]^{\frac{3}{8}} + H_3 [(T_{crit} - T_K) / T_{crit}]^{\frac{9}{4}}$. The
 219 present formulation differs from *Massman* [2012] because here $h_v(T_K \geq T_{crit}) = 0$; whereas

220 Massman's [and *Campbell's et al.* 1995] equivalent h_v was a linear approximation of the
 221 present h_v , which yielded $h_v(T_K \geq T_{crit}) \gg 0$. This distinction will become important when
 222 discussing the water vapor source term, S_v . Note that because $L_v = H_v/M_w$ it also employs
 223 Equation (8).

224 The formulations for thermal conductivity of water vapor, $\lambda_v = \lambda_v(T_K)$ [$\text{W m}^{-1} \text{K}^{-1}$],
 225 and liquid water, $\lambda_w = \lambda_w(T_K, \rho_w)$ [$\text{W m}^{-1} \text{K}^{-1}$], are taken from *Huber et al.* [2012]. For
 226 water vapor their Equation (4) is used and for liquid water the product of their Equations
 227 (4) and (5) is used. The formulations for viscosity of water vapor and liquid water are taken
 228 from *Huber et al.* [2009] and are similar algorithmically to thermal conductivity. For water
 229 vapor, $\mu_v = \mu_v(T_K)$ [$\text{kg m}^{-1} \text{s}^{-1} \equiv \text{Pa s}$], their Equation (11) is used and for liquid water,
 230 $\mu_w = \mu_w(T_K, \rho_w)$ [Pa s], their Equation (36) is used. For liquid water both these formulations
 231 include a dependence on the density of water. Consequently, once soil temperature exceeds
 232 $T_{K,max}$ both λ_w and μ_w are assigned a fixed value determined at $T_{K,max}$. On the other hand,
 233 λ_v and μ_v increase continually with increasing temperatures.

234 The formulation for the thermal conductivity of dry air, $\lambda_d = \lambda_d(T_K)$ [$\text{W m}^{-1} \text{K}^{-1}$], is
 235 Equation (5a) of *Kadoya et al.* [1985] and for the viscosity of dry air, $\mu_d = \mu_d(T_K)$ [Pa
 236 s], Equation (3a) of *Kadoya et al.* [1985] is used. The model of the thermal conductivity
 237 of soil atmosphere, $\lambda_a = \lambda_a(\lambda_v, \lambda_d, \mu_v, \mu_d)$ [$\text{W m}^{-1} \text{K}^{-1}$], is a non-linear expression given
 238 by Equation (28) of *Tsiliniris* [2008]. The relative weights used in this formulation are
 239 determined using the mixing ratios for water vapor (χ_v [*dimensionless*]) and dry air ($\chi_d =$
 240 $1 - \chi_v$): where $\chi_v = e_v/(P_d + e_v)$, and P_d [Pa] is the dry air pressure. Here P_d will be held
 241 constant and equal to the external ambient atmospheric pressure, P_{atmos} [= 92 kPa], during
 242 the laboratory experiments [see *Massman* 2012; *Campbell et al.* 1995]. The vapor pressure,
 243 e_v , is obtained from ρ_v and T_K using the ideal gas law.

244 The volumetric specific heat for soil air, $\rho_a c_{pa}$ [$\text{J m}^{-3} \text{K}^{-1}$], is estimated for the soil

245 atmosphere from $\rho_a c_{pa} = c_{pv} \rho_v + c_{pd} \rho_d$; where $\rho_d = M_d P_{atmos} / (RT_K)$ [kg m⁻³] is the dry air
 246 density, $M_d = 0.02896$ kg mol⁻¹ is the molar mass of dry air, and the isobaric specific heats
 247 for water vapor, c_{pv} [J kg⁻¹ K⁻¹], and dry air, c_{pd} [J kg⁻¹ K⁻¹], use Equation (6) of *Bücker*
 248 *et al.* [2003].

249 The saturation vapor pressure, $e_{v,sat} = e_{v,sat}(T_K)$ [Pa], and its derivative, $de_{v,sat}/dT$ [Pa
 250 K⁻¹], are modeled using Equations (2.5) and (2.5a) of *Wagner and Pruess* [2002]. The
 251 saturation vapor density, $\rho_{v,sat}$ [kg m⁻³], is modeled using Equation (2.7) of *Wagner and*
 252 *Pruess* [2002]. Following *Massman* [2012], these saturation curves are restricted to temper-
 253 atures below that temperature, $T_{K,sat}$, at which $e_{v,sat} = P_{atmos}$. For the present case $T_{K,sat}$
 254 = 370.44 K was determined from the saturation temperature equation or “the Backward
 255 Equation”, Equation (31) of *IAPWS* [2007]. For $T_K \geq T_{K,sat}$ the saturation quantities $e_{v,sat}$
 256 and $de_{v,sat}/dT$ remain fixed at their values $T_{K,sat}$, but $\rho_{v,sat}$ is allowed to decrease with in-
 257 creasing temperatures, i.e., $\rho_{v,sat} = \rho_{v,sat}(T_{K,sat}) [T_{K,sat}/T_K] [P_{atmos}/P_{ST}]$, in accordance with
 258 Table 13.2 (page 497) of *Wagner and Pruess* [2002], where $P_{ST} = 101325$ Pa is the standard
 259 pressure. The present treatment of $\rho_{v,sat}$ is different from *Massman* [2012], who assumed
 260 that $\rho_{v,sat}(T_K \geq T_{K,sat}) = \rho_{v,sat}(T_{K,sat})$.

261 Embedded in the hydraulic conductivities [K_H and K_n of Equation (2)] are the surface
 262 tension of water, $\sigma_w(T_K)$ [N m⁻¹], and the static dielectric constant (or the relative per-
 263 mittivity) of water, $\epsilon_w(T_K)$ [*dimensionless*]. These physical properties of water are integral
 264 to *Zhang’s* [2011] model for the hydraulic conductivity associated with film flow, which is
 265 incorporated into the present model and detailed in a later section. The surface tension of
 266 water is modeled following Equation (1) of *Vargaftik et al.* [1983] and $\epsilon_w(T_K)$ is taken from
 267 Equation (36) of *Fernández et al.* [1997].

268 **2.2.2 Functions Related to Water Vapor: D_{ve} , u_{v1} , S_v**

269 D_{ve} is modeled as:

$$D_{ve} = \frac{\tau(\eta - \theta)S_F\mathcal{E}D_v}{1 + e_v/P_{atmos}}$$

270 where τ [m m^{-1}] is the tortuosity of soil with $\tau = 0.66[(\eta - \theta)/\eta]^3$ after *Moldrup et al.* [1997],
 271 \mathcal{E} [*dimensionless*] is the vapor flow enhancement factor and is discussed in *Massman* [2012],
 272 $D_v/(1 + e_v/P_{atmos})$ [$\text{m}^2 \text{s}^{-1}$] is the molecular diffusivity of water vapor into the soil atmo-
 273 sphere, which will be taken as a mixture of both dry air and (potentially large amounts of)
 274 water vapor, and S_F [*dimensionless*] is Stefan correction or mass flow factor. Externalizing
 275 the $1/(1 + e_v/P_{atmos})$ term of the vapor diffusivity and combining it with S_F allows for the
 276 following approximation for $S_F/(1 + e_v/P_{atmos}) = 1/(1 - e_v^2/P_{atmos}^2) \approx 1 + e_v/P_{atmos}$; where
 277 the correct form for S_F is $1/(1 - e_v/P_{atmos})$. The reason for this approximation is to avoid di-
 278 viding by 0 as $e_v \rightarrow P_{atmos}$. *Massman* [2012] and *Campbell et al.* [1995] avoided this issue by
 279 limiting S_F to a maximum value of 10/3. This newer approximation for $S_F/(1 + e_v/P_{atmos})$
 280 is an improvement over their approach. It is relatively slower to enhance the vapor transport
 281 by diffusion than the original approach, but this is only of any real significance when $S_F \geq 1$.
 282 On the other hand because the linear form is not limited to any preset maximum value it
 283 compensates for these underestimations when $S_F > 10/3$.

284 Mindful of the externalization of $1/(1 + e_v/P_{atmos})$, D_v is estimated from the diffusivity
 285 of water vapor in dry air, $D_{vd} = D_{vd}(T_K)$ [$\text{m}^2 \text{s}^{-1}$] and the self-diffusivity of water vapor in
 286 water vapor, $D_{vv} = D_{vv}(T_K)$ [$\text{m}^2 \text{s}^{-1}$], where

$$D_{vd} = D_{vdST} \left(\frac{P_{ST}}{P_{atmos}} \right) \left(\frac{T_K}{T_{ST}} \right)^{\alpha_{vd}}$$

287 and

$$D_{vv} = D_{vvST} \left(\frac{P_{ST}}{P_{atmos}} \right) \left(\frac{T_K}{T_{ST}} \right)^{\alpha_{vv}}$$

288

289 and $T_{ST} = 273.15$ K is the standard temperature, $D_{vdST} = 2.12 \times 10^{-5} \text{ m}^2 \text{ s}^{-1}$, $\alpha_{vd} = 7/4$,
 290 $D_{vvST} = 1.39 \times 10^{-5} \text{ m}^2 \text{ s}^{-1}$, and $\alpha_{vv} = 9/4$. The parameters D_{vvST} and α_{vv} relate to the
 291 self-diffusion of water vapor and their numerical values were determined from a synthesis
 292 of results from *Hellmann et al.* [2009] and *Yoshida et al.* [2006, 2007]. The uncertainty
 293 associated with this value for D_{vvST} is at least $\pm 15\%$ and possibly more, e.g., *Miles et al.*
 294 [2012]. Blanc’s Law [*Marrero and Mason* 1972] combines D_{vd} and D_{vv} to yield the following
 295 expressions for $D_v = D_v(T_K, \rho_v)$:

$$\frac{1}{D_v(T_K, \rho_v)} = \frac{1 - \chi_v}{D_{vd}} + \frac{\chi_v}{D_{vv}} \quad \text{or} \quad D_v(T_K, \rho_v) = \frac{D_{vd}D_{vv}}{(1 - \chi_v)D_{vv} + \chi_v D_{vd}}$$

296

297 The present model for the advective velocity associated with the volatilization of water,
 298 u_{vl} , is taken from *Ki et al.* [2005] and is non-equilibrium equivalent to that used by *Massman*
 299 [2012] in his equilibrium model. Here

$$\frac{\partial u_{vl}}{\partial z} = \frac{S_v}{(\eta - \theta)\rho_v} \quad (9)$$

300

301 where the basic assumptions are that both liquid water and vapor are Newtonian fluids and
 302 that only incompressible effects are being modeled. In essence Equation (9) assumes that the
 303 vaporization of soil moisture acts as a steady-state (and rapidly expanding or “exploding”)
 304 volume source term, which yields a 1-D advective velocity associated with volatilization of
 305 liquid water. For an equilibrium model of soil moisture evaporation that does not include
 306 water movement (i.e., $K_H \equiv 0$, $K_n \equiv 0$, and $V_{\theta, surf} \equiv 0$), then $S_v \equiv -\rho_w \partial \theta / \partial t$ (from
 307 Equation (2) above), which demonstrates the connection between present model of u_{vl} with
 308 that used by *Massman’s* [2012]. But unlike *Massman* [2012], the present model does not

309 require any numerical adjustments to Equation (9) in order to maintain numerical stability.

310 The functional parameterization of S_v follows from the non-equilibrium assumption, i.e.,

311 $S_v \propto (\rho_{ve} - \rho_v)$, where $\rho_{ve} = a_w \rho_{v,sat}(T_K)$ [kg m⁻³] is the equilibrium vapor density and

312 $a_w = e^{\frac{M_w \psi_n}{RT_K}}$ [*dimensionless*] is the water activity, modeled here with the Kelvin Equation.

313 The difficult part is how to construct the proportionality coefficient. Nevertheless, there are

314 at least a two ways to go about this: (a) largely empirically [e.g., *Smits et al.* 2011 and

315 related approaches referenced therein], or (b) assume that $S_v = A_{wa} J_v$ [e.g., *Skopp* 1985

316 or *Novak* 2012], where A_{wa} [m⁻¹] is the volume-normalized soil water-air interfacial surface

317 area and J_v [kg m⁻² s⁻¹] is the flux to/from that interfacial surface. This second approach

318 allows a more physically-based parameterization of the flux, viz., $J_v = \mathcal{R}_v (\rho_{ve} - \rho_v)$, where

319 \mathcal{R}_v [ms⁻¹] is the interfacial surface transfer coefficient. For example, *Novak* [2012] proposed

320 that the flux be driven by diffusion, so that $\mathcal{R}_v = D_v / r_{ep}$, where r_{ep} [m] is the equivalent

321 pore radius and D_v is the diffusivity of water vapor in soil air. After a bit of algebra and

322 some simple geometrically-based assumptions concerning the relationships between r_{ep} , a

323 spherical pore volume, and A_{wa} , one arrives at (“the Novak”) model of the source term:

$$S_v^{[N]} = S_*^{[N]} A_{wa}^2 D_v (\rho_{ve} - \rho_v)$$

324

325 where $S_*^{[N]}$ [*dimensionless*] is an adjustable model parameter.

326 But there is another way to model the vapor flux, J_v , which is also used in the present

327 study. This second approach is based on the Hertz-Knudsen Equation, which has its origins

328 in the kinetic theory of gases and describes the net flux of a gas that is simultaneously con-

329 densing on and evaporating from a surface. A general expression for the Hertz-Knudsen flux

330 is $J_v = \sqrt{RT_K / M_w} (\mathcal{K}_e \rho_{ve} - \mathcal{K}_c \rho_v)$, where \mathcal{K}_e [*dimensionless*] is the mass accommodation (or

331 evaporation) coefficient and $\mathcal{K}_c = \mathcal{K}_c(T_K, \psi_n)$ [*dimensionless*] is the thermal accommodation

332 (or condensation) coefficient. For the present purposes $\mathcal{K}_e \equiv 1$ can be assumed. This model
 333 of J_v yields the following model for S_v :

$$S_v^{[M]} = S_*^{[M]} A_{wa} \sqrt{\frac{RT_K}{M_w}} (\rho_{ve} - \mathcal{K}_c \rho_v) \quad (10)$$

334

335 where $S_*^{[M]}$ [*dimensionless*] is an adjustable model parameter, to be determined by “tuning”
 336 it as necessary to ensure model stability. This model for $S_v^{[M]}$ is now more or less complete,
 337 but the model for $S_v^{[N]}$ is neither quite complete nor precisely comparable to $S_v^{[M]}$. This is
 338 now remedied by introducing \mathcal{K}_c into $S_v^{[N]}$ and subsuming a factor of A_{wa} into $S_*^{[N]}$, yielding:

$$S_v^{[N]} = S_*^{[N]} A_{wa} D_v (\rho_{ve} - \mathcal{K}_c \rho_v) \quad (11)$$

339

340 where $S_*^{[N]}$ [m^{-1}] now has physical dimensions, but otherwise remains an adjustable param-
 341 eter that will be scaled such that $S_v^{[N]} \approx O(S_v^{[M]})$. In this form these two models for S_v
 342 can be used to test the sensitivity of the model’s solution to different temperature forcing,
 343 because $S_v^{[M]} \propto \sqrt{T_K}$, whereas $S_v^{[N]} \propto T_K^\alpha$, where $\alpha \geq 2$.

344 Concluding the development of S_v requires models of \mathcal{K}_c and $A_{wa} = A_{wa}(\theta)$. \mathcal{K}_c is
 345 parameterized as

$$\mathcal{K}_c(T_K, \psi_n) = e^{\frac{E_{av} - M_w \psi}{R}} \left(\frac{1}{T_K} - \frac{1}{T_{K,in}} \right)$$

346

347 where $T_{K,in}$ [K] is the initial temperature of the laboratory experiments and $E_{av} - M_w \psi$
 348 [J mol $^{-1}$] is an empirically determined surface condensation/evaporation activation energy.
 349 (Note: (a) $T_K \geq T_{K,in}$, valid most of the time for any simulation, guarantees $\mathcal{K}_c \leq 1$. (b)

350 The enthalpy of vaporization, $h_v(T_K)$, is a logical choice for E_{av} ; but, model performance
351 was significantly enhanced by simply assigning a constant value for $E_{av} \approx 30 - 40 \text{ kJ mol}^{-1}$
352 rather than assigning $E_{av} \equiv h_v$.) The present formulation ensures that $\partial\mathcal{K}_c/\partial T_K < 0$, in
353 accordance with experimental and theoretical studies [*Tsuruta and Nagayama* 2004; *Kon et*
354 *al.* 2014]. Mathematically this present formulation of \mathcal{K}_c largely eliminates model instabili-
355 ties by suppressing condensation relative to evaporation throughout the experiment and will
356 be discussed in greater detail in a later section.

357 A_{wa} is parameterized as a parabolic function to simulate the conceptual model of A_{wa}
358 proposed by *Constanza-Robinson and Brusseau* [2002: see their Figure (1b)]:

$$A_{wa}(\theta) = \mathcal{S}_w(1 - \mathcal{S}_w)^{a_1} + a_2[\mathcal{S}_w(1 - \mathcal{S}_w)]^{a_3}$$

359

360 where $\mathcal{S}_w = \theta/\eta$ is the soil water saturation and $a_1 = 40$, $a_2 = 0.003$, and $a_3 = 1/8$. This
361 particular functional form ensures that $A_{wa} = 0$ when the soil is completely dry, $\theta = 0$, and
362 when fully saturated, $\mathcal{S}_w = 1$. This particular parameter value for a_1 was chosen so that
363 the maximum value of A_{wa} occurs at $\mathcal{S}_w = 0.025$ ($=1/a_1$) in accordance with the model of
364 *Constanza-Robinson and Brusseau* [2002].

365 **2.2.3 Thermal Transport Properties: C_s , λ_s**

366 The model for $C_s(T, \theta)$ is taken from *Massman* [2012]: $C_s(\theta, T) = c_s(T)\rho_b + C_w(T)\theta$,
367 where ρ_b [kg m^{-3}] is the soil bulk density; $c_s(T) = c_{s0} + c_{s1}T$ [$\text{J kg}^{-1} \text{K}^{-1}$] is the specific heat
368 capacity of soil; $C_w(T) = C_{w0} + C_{w1}T + C_{w2}T^2$ [$\text{J m}^{-3} \text{K}^{-1}$] is the volumetric heat capacity
369 of water; and the parameterization constants $c_{s0}, c_{s1}, C_{w0}, C_{w1}, C_{w2}$ are given by *Massman*
370 [2012]. Note that the present $C_s(\theta, T)$ results from approximating $C_w(T) \equiv c_{pw}(T)\rho_w(T_K)$
371 by $c_{pw}(T)\rho_w(T_{ST})$, where $c_{pw}(T)$ [$\text{J kg}^{-1} \text{K}^{-1}$] is the isobaric specific heat capacity of water,
372 and $\rho_w(T_{ST}) = 1000 \text{ kg m}^{-3}$. This substitution for $\rho_w(T_K)$ is only made for $C_w(T)$.

373 The present formulation for isobaric heat capacity of water, $c_{pw}(T)$, was developed from
374 *Yaws* [1995] and confirmed by comparing to *Wagner and Pruess* [2002]. In general $c_{pw}(T)$
375 is also a function of pressure [e.g., *Wagner and Pruess* 2002], but this dependency can
376 be ignored for the present purposes. Other parameterization of $c_{pw}(T)$ [i.e., *Sato* 1990;
377 *Jovanović et al.* 2009; *Kozłowski* 2012] were also examined, but proved unsatisfactory.
378 Finally, *Kozłowski* [2012] reports numerical values for the dry soil parameters c_{s0} and c_{s1}
379 that are similar to those discussed in *Massman* [2012] and used with the present model.

380 The model of soil thermal conductivity, λ_s , is the sum of two terms. The first, $\lambda_s^{[1]}(\theta, T_K, \rho_v)$,
381 is taken principally from *Campbell et al.* [1994] and the second, $\lambda_s^{[2]}(\theta, T_K)$, is taken from
382 *Bauer* [1993]. This second term incorporates the effects of high-temperature thermal (in-
383 frared) radiant energy transfer within the soil pore space, which may be significant for certain
384 soils and high enough temperatures [e.g., *Durany et al.* 2010]. $\lambda_s^{[1]}$ is summarized first and
385 repeated here to emphasize the difference between the present model's functional parame-
386 terizations and those used in *Massman* [2012].

387 $\lambda_s^{[1]}$ is modeled as:

$$\lambda_s^{[1]}(\theta, T_K, \rho_v) = \frac{k_w \theta \lambda_w(T_K, \rho_w) + k_a [\eta - \theta] \lambda_a^*(\theta, T_K, \rho_v) + k_m [1 - \eta] \lambda_m}{k_w \theta + k_a [\eta - \theta] + k_m [1 - \eta]} \quad (12)$$

388
389 where $\lambda_a^*(\theta, T_K, \rho_v) = \lambda_a(T_K) + \lambda_v^*(\theta, T_K, \rho_v)$ is the apparent thermal conductivity of the soil
390 air and is the sum of the thermal conductivity of moist soil air, λ_a , and λ_v^* , which incorporates
391 the effects of latent heat transfer; λ_m is the thermal conductivity of the mineral component
392 of the soil, which is assumed to be independent of temperature and soil moisture; and k_w ,
393 k_a , and k_m [dimensionless] are generalized formulations of the de Vries weighting factors
394 [de Vries 1963]. *Campbell et al.* [1994] formulate λ_v^* as proportional to the product of the
395 enthalpy of vaporization (h_v), the vapor diffusivity (D_v), the Stefan factor (S_F), the slope of

396 the saturation vapor pressure ($de_{v,sat}/dT$), and the parameter $f_w(\theta, T)$. For present model
 397 λ_v^* is

$$\lambda_v^*(\theta, T_K, \rho_v) = \frac{\hat{\rho}_{ST} h_v f_w S_F D_v [de_{v,sat}/dT]}{P_{atmos}} \quad (13)$$

398

399 where $\hat{\rho}_{ST} = 44.65 \text{ mol m}^{-3}$ is the molar density of the standard atmosphere. Equations (12)
 400 and (13) are the same as those used in *Massman* [2012], but numerically they yield quite
 401 results due to the different formulations for h_v , S_F , D_v , and $e_{v,sat} = e_{v,sat}(T_K)$. Otherwise
 402 the *de Vries* [1963] shape factors, the parameter f_w , and all related parameters are the same
 403 as in *Massman* [2012].

404 $\lambda_s^{[2]}$ is modeled as:

$$\lambda_s^{[2]}(\theta, T_K) = 3.8\sigma N^2 R_p T_K^3 \quad (14)$$

405

406 where $\sigma = 5.670 \times 10^8 \text{ W m}^{-2} \text{ K}^{-4}$ is the Boltzmann constant; $N = N(\theta) = 1 + \theta/(3\eta)$ is
 407 the medium's [*dimensionless*] index of refraction; R_p [m] is the soil's pore space volumetric
 408 radius; and the factor of 3.8 subsumes a numerical factor of 4, a [*dimensionless*] pore shape
 409 factor (= 1 for spherical particles), and the [*dimensionless*] emissivity of the medium ≈ 0.95
 410 (by assumption). In general R_p is considered to be a model parameter and it will be varied
 411 to evaluate the model's sensitivity and performance relative to $\lambda_s^{[2]}$ and unless otherwise
 412 indicated, $R_p = 10^{-3} \text{ m}$ is the nominal or default value. In the present context variations
 413 in R_p are purely model driven, but in reality such variations are likely to be most strongly
 414 associated with (or proportional to) changes in the soil particle dimensions and secondarily
 415 with other soil characteristics (e.g., *Leij et al.* 2002).

416 2.2.4 Water Retention Curve

417 In general a WRC is a functional relationship between soil moisture and soil moisture
418 potential and temperature, i.e., $\theta = \theta(\psi, T)$, although the temperature dependency is often
419 ignored and was of little consequence to *Massman's* [2012] model. The three WRCs tested
420 in the present study have been adapted to include a residual soil moisture, $\theta_r = \theta_r(\psi, T)$
421 [m^3m^{-3}], which is an atypical parameterization for both θ_r and the soil moisture's temper-
422 ature dependency. Under more normal soil environmental conditions θ_r is assumed to be
423 bound so securely to soil mineral surfaces that it is normally taken as a fixed constant. For
424 the present purposes the principal WRC is adapted from *Massman* [2012] and is

$$\theta(\psi_n, T_K) = -\frac{\theta_l}{\alpha_l} \ln(\psi_n) + \left[\theta_h - \theta_r(\psi_n, T_K) \right] \left[1 + (\alpha_h \psi_n)^4 \right]^{-\frac{1}{p}} + \theta_r(\psi_n, T_K) \quad (15)$$

425

426 Where

$$\theta_r(\psi_n, T_K) = \theta_{r*} e^{\frac{b_1 E_{av}(1-b_2\psi_n)}{R} \left(\frac{1}{T_K} - \frac{1}{T_{K,in}} \right)} \quad (16)$$

427

428 and θ_l [$\text{m}^3 \text{m}^{-3}$] is the extrapolated value of the water content when $\psi = \psi_l = -1 \text{ J kg}^{-1}$;
429 $\alpha_l = \ln(\psi_*/\psi_l) = 13.8155106$; and θ_h [$\text{m}^3 \text{m}^{-3}$], α_h [*dimensionless*] and p [*dimensionless*]
430 are parameters obtained from *Campbell and Shiozawa* [1992]; θ_{r*} [$\text{m}^3 \text{m}^{-3}$] is a constant
431 soil-specific parameter, such that $\theta_{r*} \leq 0.03$ is to be expected; and b_1 [*dimensionless*] and
432 b_2 [*dimensionless*] are adjustable parameters, which are expected to satisfy $b_1 > 0$ and
433 $0 \leq b_2 < 1$. Note: further discussion concerning the original version of Equation (15) can be
434 found in *Massman* [2012].

435 There is a simple and physically intuitive argument for the parameterization of $\theta_r(\psi_n, T_K)$
436 in Equation (16). First, under more normal soil environmental conditions, i.e., $T_K \approx T_{K,in}$
437 and at least $\psi_n < 1$ (if not $\psi_n \ll 1$), then it is reasonable to expect that $\theta_r \approx \theta_{r*}$ and

438 nearly constant throughout (what might be expected to be relatively small variations in)
 439 those conditions. But as the temperature increases, it is also reasonable to assume that
 440 the increasing amounts of thermal energy will begin to overcome the forces holding the
 441 bound water to the soil mineral surfaces and that θ_r will decrease. Mathematically, then one
 442 might therefore expect that $\partial\theta_r/\partial T_K < 0$. *Massman* [2012: see his discussion of ψ_T] made
 443 similar arguments when he included the temperature dependency in his version of the same
 444 basic WRC. Consequently, the Equations (15) and (16) above offer a different approach
 445 to including temperature effects on the WRC that maintains the temperature dependent
 446 properties of WRCs outlined by *Massman* [2012]. Second, as the temperature increases and
 447 the soil moisture (including θ_r) begins to decrease, the soil moisture potential ψ_n will begin
 448 to increase (or $\psi < 0$ will decrease in absolute terms while increasing in magnitude), which
 449 in turn (it is hypothesized) will tend to strengthen the forces holding the bound water.
 450 Therefore, one might expect that as the soil dries out $\partial\theta_r/\partial\psi_n > 0$, which will oppose,
 451 but not dominate the temperature effects (because $b_2 < 1$). Equation (16) is designed to
 452 capture these two opposing influences, assuming of course that $T_K > T_{K,in}$. But, it is itself
 453 not intended to be a fully physically-based dynamical theory of the residual soil moisture.
 454 Such a theory is beyond the intent of the present study. The sole intent here is to test
 455 and evaluate whether a dynamical θ_r can improve the model's performance. And in so far
 456 as it may succeed at doing so, it will also indicate the value and need for a more detailed
 457 physically-based dynamical model of θ_r .

458 The present study also includes similar adaptations to two other WRCs so as to test
 459 the model's sensitivity to different WRCs. These WRCs, which will not be shown here, are
 460 taken from *Groenevelt and Grant* [2004] and *Fredlund and Xing* [1994].

461 **2.2.5 Functions Related to Liquid Water Transport: \mathbf{K}_n , \mathbf{K}_H , $\mathbf{V}_{\theta,surf}$**

462 The hydraulic conductivity functions, $K_n(T_K, \psi_n, \theta)$ and $K_H(T_K, \psi_n, \theta)$, are given as fol-

463 lows:

$$K_n = \frac{K_I K_R \rho_w}{\mu_w} \psi_* \quad \text{and} \quad K_H = \frac{K_I K_R \rho_w}{\mu_w} g$$

464

465 where $g = 9.81 \text{ m s}^{-2}$ is the acceleration due to gravity; $K_I [\text{m}^2]$ is the intrinsic permeability
 466 of the soil (a constant for any given soil); and $K_R = K_R(\theta, \theta_r, \psi_n, T_K)$ [*dimensionless*] is
 467 the hydraulic conductivity function (HCF), which for the present study is taken as the sum
 468 of K_R^{cap} (associated with capillary flow) and K_R^{film} (associated with film flow). The model
 469 for intrinsic permeability, which is taken from *Bear* [1972], is $K_I = (6.17 \times 10^{-4}) d_g^2$; where
 470 d_g [m] is the mean or ‘effective’ soil particle diameter. For the soils used in the present
 471 work [*Campbell et al.* 1995; *Massman* 2012] d_g was estimated from *Shiozawa and Campbell*
 472 [1991] and *Campbell and Shiozawa* [1992] or simply assigned a reasonable value if no other
 473 information was available.

474 For present study five different parameterizations for K_R^{cap} were tested. Two were from
 475 *Grant et al.* [2010], i.e., their Equation (18) [Burdine] and Equation (19) [Mualem]; the *Van*
 476 *Genuchten and Nielson* [1985] model, their Equation(22) with the mathematical constraints
 477 imposed as suggested by *Assouline and Or* [2013]; the *Brooks and Corey* [1964] model; and
 478 Equation (18) of *Assouline* [2001]. The reason for testing several models of the HCF is to
 479 determine how different formulations for the HCF might impact the model’s performance
 480 when comparing to the laboratory observations. The following HCF is *Assouline’s* [2001]
 481 model, which is a relatively simple formulation for the HCF and serves as the reference HCF
 482 for the model simulations.

$$K_R^{cap}(\theta, \theta_r) = \left(1 - \left[1 - \left(\frac{\theta - \theta_r(\psi_n, T_K)}{\eta} \right)^{\frac{1}{m}} \right]^m \right)^n \quad (17)$$

483

484 where for the present application $0 < m < 1$, and $n > 1$.

485 $K_R^{film}(T_K, \psi_n)$ is taken from *Zhang* [2011] and is expressed, in the present notation, as:

$$K_R^{film}(T_K, \psi_n) = \frac{\mathcal{R}_w(T_K)}{6.17 \times 10^{-4}} \left[\frac{2\sigma_w}{2\sigma_w - \rho_w d_g \psi_* \psi_n} \right]^{\frac{3}{2}} \quad (18)$$

486

487 and

$$\mathcal{R}_w(T_K) = \sqrt{2} \pi^2 (1 - \eta) \mathcal{F}_w \left[\left(\frac{\epsilon_0 \epsilon_w}{2\sigma_w d_g} \right)^{\frac{1}{2}} \left(\frac{k_B T_K}{z a} \right) \right]^3 \quad (19)$$

488

489 where (section 2.2.1) $\sigma_w(T_K)$ is the surface tension of water and $\epsilon_w(T_K)$ is the static dielectric
 490 constant or relative permittivity of water; $\epsilon_0 = 8.85 \times 10^{-12} \text{ C}^2 \text{ J}^{-1} \text{ m}^{-1}$ is the permittivity of
 491 free space; $k_B = 1.308568 \times 10^{-23} \text{ J K}^{-1}$ is the Boltzmann constant; $a = 1.6021773 \times 10^{-19} \text{ C}$ is
 492 the electron charge; z [*dimensionless*] is the ion charge, for which $z = 1$ can be assumed; and
 493 \mathcal{F}_w [*dimensionless*] is a soil-specific parameter, for which *Zhang* [2011] found that (roughly)
 494 $10 < \mathcal{F}_w < 10^4$.

495 The term $\rho_w V_{\theta, surf}$ in Equation (2) represents the soil moisture movement caused by water
 496 molecules “hopping” or “skipping” along the surface of the water films due to a temperature
 497 gradient [e.g., *Medveď and Černý* 2011]. The present model for $V_{\theta, surf}$ is adapted from the
 498 model of *Gawin et al.* [1999] and is given as:

$$V_{\theta, surf} = -D_{\theta s} \frac{\partial \theta}{\partial z} = -D_{\theta s} D_{\theta \psi} \frac{\partial \psi_n}{\partial z} - D_{\theta s} D_{\theta T} \frac{\partial T}{\partial z} \quad (20)$$

499

500 where $D_{\theta s} = D_{\theta s}(T_K, \theta)$ [$\text{m}^2 \text{s}^{-1}$] is the surface diffusivity and is parameterized as:

$$D_{\theta_s} = D_{\theta_{s0}} \exp \left[-2 \left(\frac{\theta}{\theta_b} \right)^\beta \left(\frac{T_{ST}}{T_K} \right) \right] \quad (21)$$

501

502 with $D_{\theta_{s0}} \approx 10^{-10} \text{ m}^2\text{s}^{-1}$; $\theta_b \approx 0.02$; and $\beta = 1/4$ when $\theta \geq \theta_b$ or otherwise $\beta = 1$ when
 503 $\theta < \theta_b$.

504 By expressing $V_{\theta, surf}$ in terms of the gradient of the “normalized” soil moisture potential,
 505 ψ_n , in Equation (20), K_n^* and K_m , used in Equations (5) and (6), can be identified as:
 506 $K_n^* = K_n + D_{\theta_s} D_{\theta\psi}$ and $K_m = D_{\theta_s} D_{\theta T}$; where $D_{\theta_s} D_{\theta\psi}$ will be defined as K_n^{surf} ; where
 507 $K_n^{surf} \leq 0 \forall T_K$ and θ .

508 3. Numerical Implementation

509 The numerical model as outlined above and detailed in this section is coded as MATLAB
 510 (The MathWorks Inc., Natick, MA, Version R2013b) script files.

511 3.1 Crank-Nicolson Method

512 The linearized Crank-Nicolson method is used to solve Equations (5), (6), and (7). For
 513 Equation (5) this yields the following (canonical) linear finite difference equation:

$$-A_{TTi}^j T_{i-1}^{j+1} + [1 + B_{TTi}^j] T_i^{j+1} - C_{TTi}^j T_{i+1}^{j+1} + A_{T\psi i}^j \psi_{ni-1}^{j+1} - [\Gamma_{T\psi i}^j + B_{T\psi i}^j] \psi_{ni}^{j+1} + C_{T\psi i}^j \psi_{ni+1}^{j+1} =$$

514

$$A_{TTi}^j T_{i-1}^j + [1 - B_{TTi}^j] T_i^j + C_{TTi}^j T_{i+1}^j - A_{T\psi i}^j \psi_{ni-1}^j - [\Gamma_{T\psi i}^j - B_{T\psi i}^j] \psi_{ni}^j - C_{T\psi i}^j \psi_{ni+1}^j \quad (22)$$

515

516 where j and $j + 1$ are consecutive time indices, $i - 1$, i , and $i + 1$ are contiguous spatial
 517 indices, and $A_{TTi}^j, B_{TTi}^j, C_{TTi}^j, A_{T\psi i}^j, B_{T\psi i}^j, C_{T\psi i}^j$, and $\Gamma_{T\psi i}^j$ are the linearized C-N coefficients,
 518 which will not be explicitly listed here, but they do largely follow conventions and notation
 519 similar to *Massman* [2012]. Although containing more terms than Equation (22), the finite

520 difference equation corresponding to Equation (6) is very similar. But to linearize Equation
 521 (7), the Crank-Nicolson scheme requires linearizing the source term, $S_v(T, \theta, \psi, \rho_v)$. This is
 522 done with a first order Taylor series expansion of the C-N term S_v^{j+1} as follows:

$$S_{vi}^{j+1} = S_{vi}^j + \left(\frac{\delta S_v}{\delta T} \right)_i^j (T_i^{j+1} - T_i^j) + \left(\frac{\delta S_v}{\delta \psi_n} \right)_i^j (\psi_{ni}^{j+1} - \psi_{ni}^j) + \left(\frac{\partial S_v}{\partial \rho_v} \right)_i^j (\rho_{vi}^{j+1} - \rho_{vi}^j)$$

523

524 where $\frac{\delta S_v}{\delta T} = D_{\theta T} \frac{\partial S_v}{\partial \theta} + \frac{\partial S_v}{\partial T}$ and $\frac{\delta S_v}{\delta \psi_n} = D_{\theta \psi} \frac{\partial S_v}{\partial \theta} + \frac{\partial S_v}{\partial \psi_n}$, which in turn yields the following
 525 linearized finite difference equation for Equation (7):

$$\begin{aligned} & - \left[\frac{(D_{\theta T} \rho_v)_i^j}{(\eta - \theta)_i^j} + \frac{\Delta t}{2(\eta - \theta)_i^j} \left(\frac{\delta S_v}{\delta T} \right)_i^j \right] T_i^{j+1} - \left[B_{\rho \psi i}^j + \frac{\Delta t}{2(\eta - \theta)_i^j} \left(\frac{\delta S_v}{\delta \psi_n} \right)_i^j \right] \psi_{ni}^{j+1} \\ & - A_{\rho \rho i}^j \rho_{vi-1}^{j+1} + \left[1 + B_{\rho \rho i}^j - \frac{\Delta t}{2(\eta - \theta)_i^j} \left(\frac{\partial S_v}{\partial \rho_v} \right)_i^j \right] \rho_{vi}^{j+1} - C_{\rho \rho i}^j \rho_{vi+1}^{j+1} = \\ & - \left[\frac{(D_{\theta T} \rho_v)_i^j}{(\eta - \theta)_i^j} + \frac{\Delta t}{2(\eta - \theta)_i^j} \left(\frac{\delta S_v}{\delta T} \right)_i^j \right] T_i^j - \left[B_{\rho \psi i}^j + \frac{\Delta t}{2(\eta - \theta)_i^j} \left(\frac{\delta S_v}{\delta \psi_n} \right)_i^j \right] \psi_{ni}^j \\ & + A_{\rho \rho i}^j \rho_{vi-1}^j + \left[1 - B_{\rho \rho i}^j - \frac{\Delta t}{2(\eta - \theta)_i^j} \left(\frac{\partial S_v}{\partial \rho_v} \right)_i^j \right] \rho_{vi}^j + C_{\rho \rho i}^j \rho_{vi+1}^j + \frac{\Delta t}{(\eta - \theta)_i^j} S_{vi}^j \end{aligned} \quad (23)$$

526

527

528 where $B_{\rho \psi i}^j$, $A_{\rho \rho i}^j$, $B_{\rho \rho i}^j$, and $C_{\rho \rho i}^j$ are linearized C-N coefficients related to the transport terms
 529 of Equation (7) and Δt [s] is the time step. Here $\Delta t = 1.2$ s and was chosen after testing
 530 the model at $\Delta t = 0.3$ s and $\Delta t = 0.6$ s to ensure no degradation in model performance or
 531 solution stability at the larger time step.

532 **3.2 Upper Boundary Conditions**

533 The upper boundary condition on heat and vapor transfer are formulated in terms of the
 534 surface energy balance and, except for the latent heat flux, is identical to *Massman's* [2012]
 535 upper boundary condition.

$$\epsilon(\theta_0)Q_R^\downarrow(t) = \epsilon(\theta_0)\sigma T_{K0}^4 + \rho_a c_{pa} C_H [T_0 - T_{amb}(t)] + L_{v0} E_0 + G_0 \quad (24)$$

536 where the '0' subscript refers to the surface and the terms from left to right are: the incoming
 537 or down welling radiant energy, $Q_R^\downarrow(t)$ [W m^{-2}], absorbed by the surface, which is partitioned
 538 into the four terms (fluxes) on the right side of the equation, the infrared radiation lost by
 539 the surface, the surface sensible or convective heat, the surface latent heat, and the surface
 540 soil heat flux. $Q_R^\downarrow(t)$ and $T_{amb}(t)$ are functions of time and are prescribed externally as
 541 discussed in *Massman* [2012]. The soil surface emissivity, $\epsilon(\theta_0)$ [*dimensionless*], is a function
 542 of soil moisture and is taken from *Massman* [2012], as is surface heat transfer coefficient C_H
 543 [m s^{-1}]; and σ is the Stefan-Boltzmann constant.

544 The surface evaporation rate, E_0 [$\text{kg m}^{-2} \text{s}^{-1}$], is parameterized as

$$E_0 = h_{s0} C_E [\rho_{v0} - \rho_{v\text{amb}}(t)] \quad (25)$$

545
 546 where $h_{s0} \equiv a_{w0} = \exp([M_w \psi_* \psi_{n0}] / [RT_{K0}])$ [*dimensionless*] is the 'surface humidity', here
 547 modeled as the water activity at the surface using the Kelvin Equation; C_E [m s^{-1}] is the
 548 surface the transfer coefficient, an adjustable model parameter but one that can reason-
 549 ably be assumed to be between about 10^{-4} m s^{-1} [*Jacobs and Verhoef* 1997] and 10^{-3} m
 550 s^{-1} [*Massman* 2012]. Finally, in the case of the laboratory experiments of *Campbell et al.*
 551 [1995], $\rho_{v\text{amb}}(t)$, like $T_{amb}(t)$ and $Q_R^\downarrow(t)$, is an external forcing function at the soil surface.
 552 The present formulation of E_0 results from combining and adapting the expressions for the

553 potential evaporation rate for soils developed by *Jacobs and Verhoef* [1997] and Equation
 554 (9.14) of *Campbell* [1985]. For this formulation the surface relative humidity, h_{s0} , is the sur-
 555 face property that constrains or reduces the surface evaporation E_0 to less than the potential
 556 rate.

557 The upper boundary condition on soil water is $(\partial\theta/\partial z)_0 = 0$, which when employed with
 558 the WRC, Equation (15), yields the following upper boundary condition on the conservation
 559 of soil moisture, Equation (6):

$$\left(\frac{\partial\psi_n}{\partial z}\right)_0 = \left(\frac{D_{\theta T}}{D_{\theta\psi}}\right)_0 \frac{G_0}{\lambda_{s0}} \quad (26)$$

560

561 The boundary forcing functions $e_{v\,amb}(t)$ [Pa] (the ambient vapor pressure), $T_{amb}(t)$, and
 562 $Q_R^\downarrow(t)$ are taken from *Massman* [2012], which in turn were adapted to the laboratory data
 563 of *Campbell et al.* [1995]. They take the following generic form:

$$V(t) = V_i e^{-t/\tau} + V_f (1 - e^{-t/\tau})$$

564 where V_i is the value of the function at the beginning of the soil heating experiment, V_f is the
 565 value of the function at the end of the experiment, and τ [s] is a time constant of the heating
 566 source, which varies with each individual soil heating experiment. $\rho_{v\,amb}(t)$ is obtained from
 567 $e_{v\,amb}(t)$ and $T_{amb}(t)$ using the ideal gas law.

568 **3.3 Lower Boundary Conditions and Initial Conditions**

569 As with the companion model [*Massman* 2012], a numerical (or extrapolative or “pass-
 570 through”) lower boundary condition [*Thomas* 1995] is also used for the present model. An-
 571 alytically this is equivalent to assuming that the second spatial derivative ($\partial^2/\partial z^2$) of all
 572 model variables is zero at the lower boundary. It is used here for the same reason as with
 573 the previous model: principally for convenience because it is likely to be nearly impossible to

574 specify any other the lower boundary condition during a real fire. The boundary condition
575 on the advective velocity is $u_{vt} = 0$ at the bottom boundary, which is also the same as
576 with *Massman* [2012] and *Campbell et al.* [1995]. Further discussion on the model's lower
577 boundary conditions can be found in *Massman* [2012].

578 Except for the initial value of ψ_{in} (or $\psi_{n,in}$), all initial conditions (soil temperature and
579 moisture content), which are assumed to be uniform throughout the soil column for each
580 soil type and heating experiment, are taken directly from *Campbell et al.* [1995]. The initial
581 value for ψ is obtained by inverting (solving for it using) the WRC after inputting the initial
582 values for soil temperature and moisture content. Consequently, $\psi_{n,in}$ can vary with the
583 specific WRC.

584 4. Results

585 4.1 Recalibration of Observed Volumetric Soil Moisture

586 In the original soil heating experiments of *Campbell et al.* [1995] soil temperatures were
587 measured with copper-constantan thermocouples at the sample surface and at 5, 15, 25, 35,
588 65, and 95 mm depth and changes in soil moisture were obtained by gamma ray attenua-
589 tion at the same depths (except the surface). The moisture detecting system was linearly
590 calibrated for each experimental run between (a) the initial soil moisture amounts, which
591 were determined gravimetrically beforehand, and (b) the point at which the sample was
592 oven-dried (also determined before the heating experiment) where $\theta = 0$ is assumed. But
593 oven-drying a soil will not necessarily remove all the liquid water from a soil, i.e., a soil
594 can display residual water content, θ_r , after oven-drying. Consequently, the soil moisture
595 data obtained and reported by *Campbell et al.* [1995] show negative soil moistures at the
596 time the soil dryness passes outside the oven-dry range. *Massman* [2012] commented on this
597 issue. With the present study, all volumetric soil moisture data were first adjusted (using a
598 linear transformation) to rescale the observed soil moisture, $\theta_{observed}$, so that the values of

599 $\theta_{observed} < 0$ became $\theta_{observed} \approx 0$. This re-scaling had very little impact on any values of
600 $\theta_{observed}$ except those asymptotic data where $\theta_{observed} < 0$. Furthermore, this re-calibration
601 is reasonable so long as the original calibration was linear and based on a Beer's Law type
602 extinction coefficient (which would be linearly related to the logarithm of the attenuation of
603 gamma ray intensity).

604 4.2 Model Performance

605 The present model is evaluated against five of *Campbell et al.*'s [1995] soil heating exper-
606 iments: (1) Quincy Sand, which has an initial soil moisture content = $\theta_{in} = 0.14 \text{ m}^3 \text{ m}^{-3}$;
607 (2) Dry Quincy Sand with $\theta_{in} = 0.03 \text{ m}^3 \text{ m}^{-3}$, (3) Dry Palousse B with $\theta_{in} = 0.07 \text{ m}^3 \text{ m}^{-3}$,
608 (4) Wet Palousse B with $\theta_{in} = 0.17 \text{ m}^3 \text{ m}^{-3}$, and (5) Wet Boulder creek with $\theta_{in} = 0.22 \text{ m}^3$
609 m^{-3} . But here the focus is principally on Quincy Sand and Wet Palousse B. Most of the
610 major conclusions regarding the present model can be drawn from these two experiments and
611 including Quincy Sand here also benefits comparisons with *Massman* [2012], who also tested
612 his equilibrium model against the Quincy Sand data. But in addition to a general assessment
613 of model performance, these two experiments also serve as vehicles for a sensitivity analysis
614 of the key physical processes and parameterizations discussed in the previous two sections.
615 Thus, the Quincy Sand experiment is also used to explore the importance of the infrared
616 component of the soil thermal conductivity [$\lambda_s^{[2]}$: Equation (14)] and the Wet Palousse B
617 experiment is also used to evaluate the potential contribution of the dynamic residual soil
618 moisture [$\theta_r(\psi_n, T_K)$: Equations (15), (16) and (17)] to the model's performance. Finally,
619 because the HCF [Equation (17)], is central to the overall performance of the model it is
620 discussed in more detail a separate section following the Quincy Sand results.

621 4.2.1 Quincy Sand

622 Figure 1 compares the measured (symbols) and modeled (lines) of soil temperature dur-
623 ing the Quincy Sand heating experiment for two model runs with different values of R_p .

624 Increasing R_p to 4 mm (dashed lines) over the default value of 1 mm (solid lines) increases
 625 the infrared component of the soil thermal conductivity, $\lambda_s^{[2]}$. Because the model's perfor-
 626 mance was not enhanced by the inclusion of either the residual soil moisture, θ_r , or film flow,
 627 K_R^{film} , neither are included as part of the Quincy sand simulations. The colors indicate the
 628 depths (mm) of the experimental and model data. (Note: the same color is also used to
 629 denote to same depth for both the model and observed data in Figures 2, 3, and 4 below.)
 630 The corresponding measured and modeled soil moisture is shown in Figure 2. These two
 631 figures indicate that the present model produces results that are similar to both the original
 632 *Campbell et al.* (1995) model and the observations. But they also indicate that the $R_p =$
 633 4 mm simulation is superior to $R_p = 1$ mm. Furthermore, comparing these two Figures
 634 with their counterparts in *Massman* [2012] clearly indicates that the non-equilibrium model
 635 is a substantial improvement over the (older) equilibrium model, a conclusion that is easily
 636 confirmed by comparing Figures 4 through 7 below with their equivalents in *Massman* [2012].

637 Figure 3 is a plot of the data trajectory (observed soil temperatures vs observed soil
 638 moistures for all the monitored depths). The model's solution trajectories (for the same
 639 depths and the two R_p values) are shown in Figure 4. Comparing these two figures suggest
 640 that the model does a reasonable job of capturing the rapid vaporization of soil water at
 641 temperatures between 70 C and 90C (at least at the depths below about 10 mm). But the
 642 present configuration of the model does not do as well at capturing the amplitude (amount)
 643 of the recondensing moisture ahead of the rapid drying nor the duration (or width of the
 644 amplitude) of the recondensation. Furthermore, when compared with observations (Figure
 645 3) the model does not fully capture the amount of unevaporated soil moisture that remains
 646 at temperatures ≥ 150 C. In this regard neither version of the model is significantly different
 647 from the other. But some of this "lack of precision" with the soil moisture simulation results
 648 in part by how the HCF was calibrated and will be examined in more detail in the next

649 section.

650 Figure 5 compares the vertical profiles of the soil temperatures at the end of the laboratory
651 experiment with those at the end of the two numerical simulations and Figure 6 makes a
652 similar comparison for the volumetric soil moisture content. These figures also include the
653 modeling results synchronized in time and space with the observations, which are included
654 to make the model output more directly comparable to the observations. [Note: the final
655 vertical profiles obtained from the laboratory experiment are not coincident in time with the
656 measurements made at any other depth. This is a consequence of the experimental design,
657 which required several minutes to complete one vertical scan for soil moisture.] Figure 5
658 clearly indicates that the $R_p = 4$ mm simulation does a better job of capturing the final
659 temperature profile than does the $R_p = 1$ mm simulation.

660 The difference between these two model simulations is less obvious with Figure 6.
661 The final soil moisture profiles shown in this figure can be used to estimate the percentage
662 of soil moisture evaporated and lost from the soil column at the end of the 90-minute ex-
663 periment, E_{loss} . The laboratory observations suggest 31% was lost. The ($R_p = 1$ mm; red)
664 model simulation indicates a 31.4% loss and the corresponding (red) synchronized-model
665 yielded a 33.8% loss. The ($R_p = 4$ mm; blue) model simulation indicates a 34.6% loss and
666 the corresponding (blue) synchronized-model yielded a 34.2% loss. Because the fully sam-
667 pled and synchronized model results give somewhat different percentage loss it is possible
668 to conclude that the laboratory estimate of evaporative loss is likely imprecise because it is
669 poorly resolved in time and space. So exact agreement between model and observations is,
670 in general, unlikely. But it is possible to use the model itself to estimate the uncertainty in
671 the observed moisture loss that is caused by this under-sampling. This is done by comparing
672 and synthesizing all fully sampled model estimates of E_{loss} with all the corresponding syn-
673 chronized model estimates. For the five experiments studied here this uncertainty, expressed

674 as a fraction, is about ± 0.03 .

675 For the present Quincy Sand experiment this yields a fractional $E_{loss} = 0.31 \pm 0.03$, which
676 in turn suggests that both the present simulations ($R_p = 1$ mm and 4 mm) provide quite
677 good estimates of the total water loss as well as the final profiles of soil moisture and may in
678 essence really be indistinguishable. But combining these soil moisture results with the final
679 temperature profiles suggest that the $R_p = 4$ mm simulation is the preferred. In addition,
680 the present model results are significantly better than the equilibrium model, which found
681 that no water was lost during the experiment, a clearly implausible result! [Rather than
682 actually transporting the evaporated water out of the soil column, the equilibrium model
683 “pushed” the moisture deeper into the soil ahead of the evaporative front as discussed in the
684 Introduction.] On the other hand, despite the fact that the present estimates of evaporative
685 loss are clearly a major improvement over the equilibrium results, both the equilibrium and
686 non-equilibrium model solutions produce a sharply delineated advancing drying front, which
687 is reminiscent of a Stefan-like or moving-boundary condition problem (e.g., see *Whitaker*
688 *and Chou* 1983-1984 or *Liu et al.* 2005). So neither simulation actually captures the final
689 observed moisture profile behind the drying front.

690 Figure 7 shows the final (90-minute) modeled profiles of (a) the ($R_p = 1$ mm) soil vapor
691 density $[\rho_v(z)]$, equilibrium vapor density $[\rho_{ve}(z)]$, and the condensation term $[\mathcal{K}_c(z)\rho_v(z)]$,
692 used with the non-equilibrium model source term, S_v : Equations (10) and (11)] and (b)
693 the ($R_p = 4$ mm) soil vapor density $[\rho_v(z)]$. The solid lines are model simulations with R_p
694 = 1 mm; the dashed red line corresponds to the $R_p = 4$ mm simulation. (For the sake of
695 simplicity only one curve is shown for $R_p = 4$ mm simulation.) The maximum soil vapor
696 density occurs at about 40 mm where the evaporative source term is greatest, i.e., where
697 $\rho_{ve}(z) - \mathcal{K}_c(z)\rho_v(z)$ is maximal, and where the moisture gradient is steepest, which is just
698 ahead of the drying front (Figure 6). Furthermore, the ρ_v profile suggests that there are both

699 upward and downward diffusional fluxes of vapor away from the maximal evaporative source.
700 The upward-directed flux escapes through the soil surface and into the ambient environment
701 of the laboratory (the surface evaporative flux) and the downward-directed flux eventually
702 recondenses below of the dry front. The equilibrium model, on the other hand, produced
703 virtually no vapor gradient within the dry zone thereby contributing to the model's inability
704 to allow any moisture to escape (evaporate) from the modeling domain. Unfortunately, there
705 are no observations with which to check either models' predictions of vapor density. But,
706 although both models' results tend to agree that within the dry zone where temperatures
707 exceed the critical temperature for water (= 373.95 C) there should be a single phase fluid
708 that is significantly denser than water vapor near STP (e.g., *Pakala and Plumb* 2012), the
709 non-equilibrium model does predict a more realistic vapor gradient than the non-equilibrium
710 model.

711 If there is an implausibility with the present model it might be the soil vapor pressure,
712 e_v , as shown in Figure 8. With either model simulation e_v at the top of the soil column
713 is between about 3 standard atmospheres (≈ 300 kPa). This is a bit unexpected because
714 pressure at the open end of the column might be expected (at least by this author) to be close
715 to equilibrium with the ambient pressure (≈ 92 kPa). Although there are no data against
716 which to check this result, there are other modeling results that lend some support to the
717 present predictions for e_v . First, (Figure 5 of) *Udell's* [1983] steady state model of a sand-
718 water-steam system heated from above indicates that the environment within the modeling
719 domain is likely to be super-saturated and that at a minimum e_v is greater than P_{atmos}
720 by $\approx 5\%$, but (depending on the algorithmic treatment of the saturation vapor pressure
721 and the exact value of P_{atmos} he used for his simulations) it is also plausible to expect that
722 $e_v \approx (2 - 5)P_{ST}$. (Note that for *Udell's* [1983] simulations the maximum model temperature
723 was about 180 C and that he also modeled advective velocity using Darcy's law.) Second,

724 two different models of heated cement [Dayan 1982 and Dal Pont et al. 2011] indicate that
725 near the top surface of the model domain e_v can display values of $\approx (2 - 15)P_{ST}$. The overall
726 similarities between these three earlier models and the present non-equilibrium model make
727 it impossible to completely invalidate the present model's predictions for e_v . Furthermore,
728 the non-equilibrium model imposes no particular constraint on e_v – it is calculated using
729 the ideal gas law and the profiles of vapor density and temperature, both of which appear
730 plausible. Consequently, the somewhat surprising result shown in Figure 8 appears to be a
731 natural consequence of the physics underlying the basic model equations: the conservation
732 of mass and thermal energy.

733 4.2.2 HCF – Quincy Sand

734 Figure 9 shows the hydraulic functions K_H^{cap} , K_H^{film} , $|K_n^*|$, $|K_n|$, and $|K_n^{surf}|$ as functions
735 of soil moisture for the model simulation with $R_p = 1$ mm. (Recall that the components
736 of the hydraulic diffusivity are all negative, so this figure reflects only their absolute value,
737 not their sign). K_H^{film} [assuming $\mathcal{F}_w = 10^3$, Equation (19)] was calculated after the model
738 run using the model's solution for T_K , θ , and ψ . Because K_H^{film} did not actually contribute
739 anything to any of the model runs for any of the five soil heating experiments (even for $\mathcal{F}_w =$
740 10^4), the present approach for evaluating it is sufficient. Consequently although $|K_n|$ shown
741 here is more properly termed $|K_n^{cap}|$, this distinction is rendered moot for the present study.
742 The values for m and n of K_R^{cap} , Equation (17), were $m = 0.26$ and $n = 1.80$ and were
743 obtained by subjectively optimizing the model (with $R_p = 1$ mm) to fit the data shown in
744 Figures 1, 2, 5, and 6. In other words, it is possible to improve the model's performance for
745 either the temperature data or the soil moisture data individually, but not simultaneously.
746 Any improvement in one set of observations (T_K or θ) comes at the expense of the model's
747 performance for the other variable. As a consequence of this optimization the model's ability
748 to fully capture the amplitude (amount) of soil moisture that evaporates and recondenses

749 ahead of the drying front [Figures 3 and 4] has been sacrificed to improve the simulation of
750 the soil temperatures. So the present numerical solution is a compromise between trying to
751 fit two sets of data with a single “best” parameterization of *Assouline’s* [2009] K_R^{cap} . Similar
752 compromises were required for other heating experiments as well. These particular optimal
753 values for m and n were also found valid for the Boulder creek soil experiments; but for the
754 Palouise B soil the optimal values were $m = 0.29$ and $n = 1.82$.

755 Unfortunately, there are no independent confirmations for any values of m and n because
756 no soil hydraulic conductivity data were (or ever have been) obtained for any of the soil
757 samples used by *Campbell et al.* [1995]. Nor are any data likely at this point in time because
758 the original samples were destroyed years ago (*G. S. Campbell*, personal communication,
759 2015). At the time of these laboratory experiments the basic assumption that the original
760 researchers made was that the heating and evaporation rates would be so fast as to preclude
761 any (presumably much slower) liquid water transport associated with gradients in soil water
762 potential. The present results appear to invalidate that assumption.

763 Although it is undeniably true that the present model is an improvement over the equi-
764 librium model, the inclusion of the HCF within this non-equilibrium model (and its lack of
765 inclusion in the equilibrium model) makes it difficult to conclude unambiguously that the
766 improvement over equilibrium model is the sole consequence of the non-equilibrium assump-
767 tion. But the non-equilibrium model was tested in a mode that basically “turned off” K_R
768 and reduced K_n^{surf} by several orders of magnitude and still it yielded a solution (not shown)
769 that simulated the soil temperatures and soil moisture observations better than did the equi-
770 librium model. Furthermore, the non-equilibrium assumption will always remain superior to
771 the equilibrium assumption for dry or extremely dry soils. Nonetheless, it remains unknown
772 how much, if any, improvement in the equilibrium model’s performance is possible with the
773 inclusion of a HCF.

774 Finally it should also be pointed out that, unlike K_R^{film} , K_n^{surf} does contribute positively
775 and significantly to the present model's performance because without it the model can be-
776 come unstable for very dry soils. Therefore, K_n^{surf} is a significant factor in the HCF's overall
777 contribution to the performance of the non-equilibrium model.

778 4.2.3 Wet Palousse B

779 Figure 10 compares the measured (symbols) and modeled (lines) of soil temperatures
780 during the Wet Palousse B heating experiment with the model run that includes the residual
781 soil moisture, θ_r (dashed), and that which does not (solid). Figure 11 compares the measured
782 (symbols) and modeled (lines) of soil moisture during the same experiment. Figure 12 shows
783 the two models' solution trajectories, where the dashed line is the model run that includes
784 θ_r and the solid line does not. These results suggest that the inclusion of the θ_r in the model
785 does not influence temperatures very much, but that the soil moisture dynamics are much
786 better portrayed by the model with θ_r than without it. In fact, the main difference between
787 these two simulations is that the soil moisture that evaporates and recondenses ahead of the
788 drying front is much less for the model that includes θ_r than that which does not (Figure
789 12). The significance of this aspect of the model's performance is demonstrated in Figure 13,
790 which, by comparing the observed Palousse B Wet trajectory data with the data from the
791 θ_r -configured model, demonstrates that the θ_r -configured model reproduces the observations
792 far more closely than does the model configured without θ_r . The next two figures, Figures
793 14 and 15, compare the final modeled and observed profiles of temperature and moisture
794 for the Wet Palousse B experiment. These last two figures demonstrate (even more clearly
795 than the previous figures) that including the dynamic soil moisture, θ_r , has very little effect
796 on the modeled soil temperatures, but that it does have a significant and positive effect on
797 the modeled soil moistures. The predicted soil water loss from the θ_r -configured model is
798 almost exactly in agreement with the observed value of 28.8% and the modeled moisture

799 profile below the drying front is also in almost perfect agreement with the observed data.
800 The model without θ_r allows much more evaporated moisture to diffuse downward and to
801 recondense ahead of the drying front than does the θ_r model; thereby underestimating the
802 water loss by about half and significantly overestimating the amount of soil water in lower
803 portion of the profile.

804 **4.3 Further Sensitivity Analyses**

805 The Quincy Sand and Palousse B results in general confirm that the non-equilibrium
806 model's performance is enhanced (and quite significantly) with the incorporation of liquid
807 water transport (HCF) and that its performance is sensitive to (and can be improved by)
808 either or both (a) the infrared thermal conductivity, $\lambda_s^{[2]}$, through the volumetric pore radius,
809 R_p , and (b) the dynamical residual soil moisture, $\theta_r(\psi, T_K)$. Although these last two aspects
810 of the present model may not apply equally to any given soil, there seems little doubt that
811 they should be considered as potentially quite important for modeling soil moisture and
812 temperature dynamics during heating of soil during fires.

813 The remainder of this section is a summary of various (secondary, but important) model
814 sensitivity analyses performed with all soil heating experiments. The ultimate intent here is
815 to shed light on which physical process are relatively more important and to provide some
816 guidance for further research.

817 **4.3.1 The Source Term, Thermal Conductivity, and Surface Evaporation**

818 Central to the success of the present model, relative to the performance of the equilibrium
819 model of *Massman* (2012), is the functional parameterization of the source term, S_v , and the
820 related condensation coefficient, $\mathcal{K}_c(T_K, \psi_n)$. Basically \mathcal{K}_c was required to maintain model
821 stability especially at high temperatures; without it the model was unstable and the dynamic
822 between moisture and vapor was non-physical. Regarding \mathcal{K}_c , the model is weakly sensitive
823 to the choice of the surface evaporation/condensation activation energy, E_{av} , providing it

824 does not vary much outside the range of $30 \text{ kJ mol}^{-1} \leq E_{av} \leq 40 \text{ kJ mol}^{-1}$. On the other
 825 hand, from a systems perspective it is very difficult to infer much about the details of the
 826 (high-temperature) physical processes associated with \mathcal{K}_c or of the generality/universality
 827 of E_{av} , other than their apparent existence and utility to the present model. The most
 828 effective value for the scaling parameter, $S_*^{[M]}$, was within the range of about 0.5 to 1.
 829 The Novak model of the source term, $S_v^{[N]}$, also required the same \mathcal{K}_c , but the additional
 830 temperature dependency of $S_v^{[N]}$ over $S_v^{[M]}$ forced the soil moisture to evaporate at slightly
 831 lower temperatures (therefore sooner) than shown in Figure 4 for the Quincy Sand $S_v^{[M]}$ -
 832 configured model. $S_v^{[N]}$ also eliminated an initial transient/instability (not shown) that
 833 occurred with the Quincy Sand $S_v^{[M]}$ solution. Otherwise, the differences between $S_v^{[N]}$ and
 834 $S_v^{[M]}$ were not significant.

835 It should not be surprising that the model is sensitive to soil thermal conductivity, λ_s ; but
 836 it was somewhat surprising that the model is as sensitive to $\lambda_s^{[2]} [R_p]$ as it is. Both *Durany*
 837 *et al.* [2010] and *Massman* [2102] found that $\lambda_s^{[2]}$ only contributed for relatively porous soils,
 838 i.e., $R_p > 10^{-3} \text{ m}$. In the present study the model temperatures could often be “fine tuned”
 839 (improved) even for relatively small values of R_p . Therefore, in general, it seems unwise to
 840 ignore $\lambda_s^{[2]}$, at least when modeling soil heating during fires.

841 The most important parameter controlling surface evaporation rate is the surface transfer
 842 coefficient C_E , to which the model is reasonably sensitive. In particular (and similar to
 843 *Massman*’s 2012 results), the best values of C_E were universally about 10^{-3} m s^{-1} and
 844 values much above this caused the model to become unstable. Values well below these
 845 values (and closer to the theoretical value of 10^{-4} m s^{-1}) did not produce results much
 846 different than those resulting from $C_E = 10^{-3} \text{ m s}^{-1}$. Nevertheless, C_E does play a weak role
 847 in determining the soil surface temperature, T_{K0} , and therefore can influence the magnitude
 848 of the surface convective heat flux – Equation (24) – and $\lambda_{s0}^{[2]}(T_{K0})$, which can influence the

849 soil temperatures to some depth below the soil surface.

850 4.3.2 Water Retention Curves and Hydraulic Conductivity Functions

851 The two other WRCs tested for model performance were *Groenevelt and Grant* [2004]
852 (GG04) and *Fredlund and Xing* [1994] (FX94). But prior to implementing them in the model
853 they were both calibrated to be numerically similar near the dry end ($\theta \leq 0.03$) of Equation
854 (15). Their performance was initially tested with the *Assouline* [2009] HCF, Equation (17).
855 In addition, and as listed in section 2.2.5, besides Equation (17) four other HCFs were also
856 tested. Although not all pairings of WRCs and HCFs were tested against every heating ex-
857 periment, the following conclusions seem relatively robust: (1) once calibrated to the present
858 data set, the *Brooks and Corey* [1964] HCF performed at least as well as Equation (17), but
859 with only one parameter rather than two, while the other three HCFs gave somewhat less
860 satisfying results and sometimes would even produce an instability; (2) the FX94 WRC often
861 produced an instability, but its performance was also somewhat dependent upon which HCF
862 was used with it; and (3) the GG04 WRC and associated HCFs did perform better the FX94,
863 but overall, it did not perform as well as the present model configuration with Equation (15)
864 for the WRC and Equation (17) for the HCF. In general the only guidance offered here is
865 that some care must be given to choice of WRCs and HCFs because the modeling results
866 can be quite dependent upon the choices made.

867 Universal to all of HCFs tested here is K_n^{surf} [i.e., $V_{\theta, surf}$ and its scaling parameter $D_{\theta s0}$:
868 see Equations (20) and (21)], which as explained above was incorporated into the hydraulic
869 diffusivity, K_n^* [see Equation (6) and the related discussion]. The model’s performance was
870 relatively insensitive to the exact value of $D_{\theta s0}$ and $D_{\theta s0} \approx 10^{-10} \text{ m}^2\text{s}^{-1}$ is as good a default
871 value as any other value. Furthermore, the inclusion of $V_{\theta, surf}$ (soil moisture movement
872 associated with water molecules “hopping or skipping” along the soil and water surfaces)
873 did provide model stability when the soil moisture reached extremely low values. Including

874 film flow, K_r^{film} – Equations (18) and (19), brought no discernible benefit to the model’s
875 performance. For less extreme conditions and for relatively coarse-grained sand *Smits et*
876 *al.* [2012] reached a similar conclusion. Nonetheless, K_r^{film} should not be discounted as
877 unimportant, so further investigation into it’s utility for modeling still seems warranted.

878 4.3.3 Different Soils with Different Initial Conditions

879 Of the remaining three heating experiments only Wet Boulder creek, which had an initial
880 soil saturation level of about 50%, showed anything unexpected. In general, the model was
881 able to capture the observed soil temperatures and temperature dynamics extremely well,
882 even better than shown in either Figure 5 (Quincy Sand) or Figure 14 (Palousse B). But,
883 regardless of any adjustments to any of the model parameters the model consistently under-
884 estimated the total amount of water evaporated (by about half), thereby also overestimating
885 the amount of recondensing water ahead of the drying front (see the Wet Palousse B model
886 run without θ_r , Figure 15, as an example). On the other hand, the model was able to capture
887 the complete drying ($\theta \equiv 0$) of the top 30 mm of the soil column during the Wet Boulder creek
888 experiment, whereas the Quincy Sand (Figure 6) and Palousse B (Figure 15) experiments
889 indicated some residual soil moisture ($0 < \theta < 0.025$) within the model’s predicted dry zone.
890 The model’s performance was noticeably degraded when θ_r was included and it was also
891 quite sensitive to the choice of R_p , so much so that best model fit to temperatures required
892 that $R_p = 0$, i.e., that $\lambda_s^{[2]}$ be excluded from the model. Nonetheless, the cause for this
893 unexpected divergence between the modeling and observed soil moisture during this heating
894 experiment is not understood. For the present it can only be surmised that the model’s
895 description of evaporative dynamics of soil moisture, and possibly the transport of water
896 (both liquid and vapor), is still incomplete.

897 4.3.4 The advective velocity, \mathbf{u}_v

898 Unlike with the companion model [*Massman* 2012], the present model did not require

899 reducing the magnitude of u_{vl} in order to maintain model stability, which again reinforces
900 the impression that the present non-equilibrium model is an improvement over equilibrium
901 model. Nonetheless, the present model can produce extraordinary gradients of vapor density
902 and vapor pressure, which begs the question of whether such gradients could induce other
903 types of mass transport than that captured by the present formulation of u_{vl} , Equation
904 (9). This was tested by using a model for Darcy’s Law type formulation based on the
905 assumption that the advective velocity is proportional to the vapor pressure gradient ($u_{vl} \propto$
906 $-\partial e_v/\partial z$). This formulation was tested by incorporating it into the model (excluding θ_r).
907 But the model became unstable because mathematically it was strongly hyperbolic, rather
908 than predominantly parabolic. Further modeling development and parameterization of u_{vl}
909 and vapor transport in general are well beyond the intent of the present study. But it is
910 still possible to conclude that such exploration is warranted and could help improve model
911 performance. Finally, it should be noted that the model’s performance was degraded when
912 u_{vl} was excluded from the model.

913 4.3.5 Different forms of Fick’s First Law for the diffusive flux

914 The point was made earlier that the present model was developed assuming the mass form
915 for the diffusive flux, i.e., $J_{diff}^{[Mass]} = -D_{ve}\partial\rho_v/\partial z$; but that there are other forms that could
916 have been used. Most notable among them is likely to be the mass fraction form for Fick’s
917 First Law: $J_{diff}^{[Fraction]} = -D_{ve}(\rho_v + \rho_d)\partial\omega_v/\partial z$. But $J_{diff}^{[Pressure]} = -D_{ve}[M_w/(RT_K)]\partial e_v/\partial z$
918 was also previously mentioned and was used by *Campbell et al.* [1995]. Implementing either
919 of these latter two forms of Fick’s Law requires amending $J_{diff}^{[Mass]}$ to include the influence
920 of the temperature gradient on the diffusive flux. This is most easily accomplished with
921 $J_{diff}^{[Pressure]}$ by combining it with the ideal gas law for water vapor, $e_v = \rho_v RT_K/M_w$, to yield:

$$J_{diff}^{[Pressure]} = -D_{ve} \left[\frac{M_w}{RT_K} \right] \frac{\partial e_v}{\partial z} = -D_{ve} \frac{\partial \rho_v}{\partial z} - D_{ve} \left[\frac{\rho_v}{T_K} \right] \frac{\partial T}{\partial z} = J_{diff}^{[Mass]} - D_{ve} \left[\frac{\rho_v}{T_K} \right] \frac{\partial T}{\partial z} \quad (27)$$

922

923 A similar result is produced for $J_{diff}^{[Fraction]}$ by combining it with the ideal gas law for
 924 the dry air component of the soil pore space air, $\rho_d = P_d RT_K / M_d$, with the understanding
 925 that $P_d = P_{atmos}$ is held constant because P_{atmos} , the external ambient atmospheric pressure
 926 during the time of the experiment, is constant and not influenced by changes in vapor
 927 pressure within the soil column during the soil heating experiment. The final expression for
 928 $J_{diff}^{[Fraction]}$ is:

$$\begin{aligned}
 J_{diff}^{[Fraction]} &= -D_{ve}(\rho_v + \rho_d) \frac{\partial}{\partial z} \left[\frac{\rho_v}{\rho_v + \rho_d} \right] = -\frac{D_{ve}}{(1 + \rho_v/\rho_d)} \left[\frac{\partial \rho_v}{\partial z} - \frac{\rho_v}{\rho_d} \frac{\partial \rho_d}{\partial z} \right] = \\
 &= \frac{J_{diff}^{[Mass]}}{(1 + \rho_v/\rho_d)} - \frac{D_{ve}}{(1 + \rho_v/\rho_d)} \left[\frac{\rho_v}{T_K} \right] \frac{\partial T}{\partial z} = \frac{J_{diff}^{[Pressure]}}{(1 + \rho_v/\rho_d)} \quad (28)
 \end{aligned}$$

929

930

931 Comparing Equations (27) and (28) shows that except for the $(1 + \rho_v/\rho_d)$ term in the
 932 denominator of $J_{diff}^{[Fraction]}$ these two expressions for J_{diff} are the same. For the purposes of
 933 the sensitivity test both Equations (27) and (28) were used with ρ_v as the predicted variable
 934 (i.e., ρ_{vi}^{j+1} and ρ_{vi}^j are the Crank-Nicolson finite difference variables) and T as the model
 935 variable for the linearized coefficients (i.e., T_i^j). The resulting finite difference terms were
 936 implemented into Equation (23) and into the finite difference equivalent of Equation (6).

937 None of the model solutions resulting from either $J_{diff}^{[Fraction]}$ or $J_{diff}^{[Pressure]}$ were useful.
 938 They were all either (a) unstable or (b), if stable, physically unrealistic. In other words, no
 939 solution associated with either of these other two forms of J_{diff} could be found that was
 940 not largely meaningless when compared to the observations. Consequently, the only possible
 941 conclusion here is that no improvement to the present model's performance is possible when
 942 using either $J_{diff}^{[Fraction]}$ or $J_{diff}^{[Pressure]}$. This in turn supports the notion that for the physical

943 problem considered in the present study $J_{diff}^{[Mass]}$ appears to be the preferred expression for
944 J_{diff} .

945 5. Summary and Recommendations

946 This study has developed and tested a non-equilibrium (liquid to vapor phase change)
947 model for simulating heat and moisture flow in soils during fires; but the model does assume
948 thermal equilibrium. By and large the simulations of soil temperature and moisture are
949 not only credible, but often quite good. In general, all model results showed a significant
950 improvement over all comparable results from the companion equilibrium model of *Massman*
951 [2012].

952 The principal reason for the present model's success is the incorporation of a dynamic
953 condensation coefficient, \mathcal{K}_c (parameterized as a function of temperature and soil water po-
954 tential), into the non-equilibrium evaporative source term, S_v ; both of which are modeled
955 after the Hertz-Knudsen Equation. Physically \mathcal{K}_c suppressed condensation in favor of evapo-
956 ration at high temperatures and soil water potentials, which in turn insured model stability.
957 Furthermore, the non-equilibrium assumption also seemed to have improved the parameter-
958 ization (and performance) of the mass transport associated with the advective velocity, u_{vl} ,
959 relative to the model's of *Massman* [2012] and *Campbell et al.* [1995]. The model's perfor-
960 mance was further and significantly enhanced by the inclusion of a hydraulic conductivity
961 function (HCF) for liquid water transport, which was calibrated here by "fitting" the HCF
962 parameters to ensure that the model optimally reproduced the observed temperature and
963 moisture dynamics. This fitting procedure was necessary because no data are (nor will be)
964 available for the soil samples used in the laboratory heating experiments [*Campbell et al.*
965 1995]. Another important (and novel) feature of the model is the inclusion of a dynamic
966 residual soil moisture θ_r , also parameterized as a function of temperature and soil water po-
967 tential, which is introduced into the model in an attempt to capture the long evaporative tail

968 that seems to require temperatures well beyond 100 C in order to evaporate at all. Physically
969 θ_r is intended to represent the strongly bound soil moisture, which for the present purposes
970 is conceptualized as a mono-layer. Including θ_r was sometimes, but not always, beneficial
971 to model performance. So it seems worthy of further consideration and possible refinement
972 in any future studies of a similar nature. Finally, the model is also sensitive to the thermal
973 infrared radiation component to the soil's thermal conductivity [$\lambda_s^{[2]}$: Equation (14)], which
974 increases the thermal conductivity within the pore space of the soil as temperature increases.
975 It is recommended that this term also be included and further tested when evaluating any
976 future models describing the heating soils to high temperatures.

977 In general, the model simulates the observed soil temperatures quite well. It is often
978 slightly less precise for soil moisture and the best simulations were usually a compromise
979 between faithfully representing the observed soil temperatures or the observed soil moistures.
980 Nonetheless, the model does capture reasonably well many observed features of the soil
981 moisture dynamics, viz., it simulates an increase in soil moisture ahead of the drying front
982 (due to the condensation of evaporated soil water at the front) and the hiatus in the soil
983 temperature rise during the strongly evaporative stage of the soil drying. Furthermore, the
984 model also captures the observed rapid evaporation of soil moisture that occurs at relatively
985 low temperatures (50-90 C), as well as some aspects of the long evaporative tail associated
986 with strongly bound soil moisture. But, the model also displays a tendency to predict a
987 greater depth of the drying front than suggested by the observations.

988 Sensitivity analyses (SAs) were also performed with different formulations for the water
989 retention curve, soil hydraulic conductivity function, one variant of the present evaporative
990 source term, S_v , and different soil types with different initial conditions. The principal
991 conclusion from these SAs is that some care (and testing) must be given to the selection of
992 the WRC and HCF, as not all of them performed equally well. Some further investigations

993 into the modeling benefit of film flow as part of the HCF also seems warranted. The two
994 forms of S_v tested here performed about the same. And the model's performance (at least for
995 soil moisture) was poorest compared to the experiment with the highest initial soil moisture
996 content. No obvious explanation for this 'under-performance' could be found, so it seems
997 worthwhile to further test the model for high initial saturation conditions. Finally, it is
998 important to test the present model's performance and its associated parameterizations
999 (particularly the WRC and HCF) against laboratory data and field data associated with
1000 daily cycles of soil heating and moisture transport.

1001 **Acknowledgments**

1002 All modeling code and data used in this paper are freely available from the author.
1003 I would like to thank Gaylon S. Campbell for providing the laboratory data used in this
1004 study, as well as James W. Thomas for his insights into and discussions of the mathematical
1005 and numerical issues I encountered during the development of this model and Marcia L.
1006 Huber and Allan H. Harvey for various discussions concerning the thermophysical properties
1007 of water and aid with the published resources used in parameterizing the self diffusion of
1008 water vapor.

References

- [1] Assouline, S.: A model for the relative hydraulic conductivity based on the water retention curve, *Water Resour. Res.*, 37, 265-271, 2001.
- [2] Assouline, S. and Or, D.: Conceptual and parametric representation of hydraulic properties: A review, *Vadose Zone Journal*, 12, 1-20, doi:10.2136/vzj2013.07.0121, 2013.
- [3] Aston, A. R. and Gill, A. M.: Coupled soil moisture, heat and water vapour transfers under simulated fire conditions, *Australian J. Soil Res.*, 14, 55-66, 1976.
- [4] Bauer, T. H.: A general analytical approach toward the thermal conductivity of porous media, *Int. J. Heat Mass Transfer*, 36, 4181-4191, 1993.
- [5] Bear, J.: *Dynamics of Fluids in Porous Media*, American Elsevier Pub. Co, New York, NY, USA, 1972.
- [6] Bridge, L., Bradean, R., Ward, M. J., and Wetton, B. R.: The analysis of a two-phase zone with condensation in a porous medium, *J. Eng. Math.*, 45, 247-268, 2003.
- [7] Brooks, R. H. and Corey, A. T.: *Hydraulic properties of porous media*, Hydrology Paper 3, Colorado State University, Fort Collins, CO, USA, 1964.
- [8] Bücker, D., Span, R., and Wagner W.: Thermodynamic property models for moist air and combustion gases, *J. Eng. Gas Turbines Power*, 125, 374-384, 2003.
- [9] Campbell, G. S.: *Soil Physics with BASIC*, Elsevier, New York, NY, USA, 1985.
- [10] Campbell, G. S., Jungbauer Jr., J. D., Bidlake, W. R., and Hungerford, R. D.: Predicting the effect of temperature on soil thermal conductivity, *Soil Science*, 158, 307-313, 1994.

- 1030 [11] Campbell, G. S., Jungbauer Jr., J. D., Bristow, K. L., and Hungerford, R. D.: Soil
1031 temperature and water content beneath a surface fire, *Soil Science*, 159, 363-374, 1995.
- 1032 [12] Campbell, G. S., and Shiozawa, S.: Prediction of hydraulic properties of soils using
1033 particle-size distribution and bulk density data, in *Indirect methods for estimating the*
1034 *hydraulic properties of unsaturated soils*, edited by M. Th. van Genuchten, University
1035 of California, Riverside, CA, 317-328, 1992.
- 1036 [13] Costa, V. A. F., Mendoça M. L., and Figueiredo, A. R.: Modeling and simulation of
1037 wetted porous thermal barriers operating under high temperature or high heat flux,
1038 *Int. J. Heat Mass Trans.*, 51, 3342-3354, 2008.
- 1039 [14] Constanza-Robinson, M. S., and Brusseau, M. L.: Air-water interfacial areas in un-
1040 saturated soils: evaluation of interfacial domains, *Water Resour. Res.*, 38 (10), 1195,
1041 doi:10.1029/2001WR000738, 2002.
- 1042 [15] Cowan, I. R.: Stomatal behavior and environment, in *Advances in Botanical Research*,
1043 edited by R. D. Preston and H. W. Woolhouse, Academic Press, London, UK, 117-229,
1044 1977.
- 1045 [16] Dal Pont, S., Meftah, F., and Schrefler, B. A.: Modeling concrete under severe condi-
1046 tions as a multiphase material, *Nuclear Engineering and Design*, 241, 562-572, 2011.
- 1047 [17] Danielewicz-Ferchmin, I., and Mickiewicz, A. R.: Water Density in the Double Layer,
1048 *J. Phys. Chem.*, 100, 17281-17286, 1996.
- 1049 [18] Dayan, A.: Self-similar temperature, pressure and moisture distribution within an
1050 intensely heated porous half space, *J. Heat Trans.*, 25, 1469-1476, 1982.

- 1051 [19] de Vries, D. A.: Simultaneous transfer of heat and moisture in porous media, EOS
1052 Trans. AGU, 39, 909-916, 1958.
- 1053 [20] de Vries, D. A.: Thermal properties in soils, in Physics of Plant Environment, edited
1054 by W. R. van Wijk, North Holland Publishing Co., Amsterdam, 201-255, 1963.
- 1055 [21] di Blasi, C.: Simultaneous heat, mass, and momentum transfer during biomass drying,
1056 in Developments in Thermochemical Biomass Conversion, edited by A. V. Bridgwater
1057 and D.G.B. Boocock, Springer Science+Business Media, Dordrecht, 117-131, 1997.
- 1058 [22] Durany, J., Fraga, B., and Vargas, F.: Physical modelling and numerical simulation
1059 of soil heating under forest fire conditions, in Forest Fire Research, edited by D. X.
1060 Viegas, ADAI/CEIF, Coimbra, Portugal, paper no. 263 of the attached CD, 2010.
- 1061 [23] Fernández, D. P., Goodwin, A. R. H., Lemmon, E. W., Levelt Sengers, J. M. H. and
1062 Williams, R. C.: A Formulation for the static permittivity of water and steam at
1063 temperatures from 238 K to 873 K at pressures up to 1200 MPa, including derivatives
1064 and Debye-Hückel coefficients, J. Phys. Chem. Ref. Data, 26, 1125-1166, 1997.
- 1065 [24] Fredlund, D. G. and Xing, A: Equations for the soil-water characteristic curve, Can.
1066 Geotech. J., 31, 521-532, 1994.
- 1067 [25] Gawin, D., Majorana, C. E., and Schrefler, B. A.: Numerical analysis of hydro-thermal
1068 behavior and damage of concrete at high temperatures, Mech. Cohes.-Frict. Materials,
1069 4, 37-74, 1999.
- 1070 [26] Grant, C. D., Groenevelt, P. H., and Robinson, N. I.: Application of the Grant-
1071 Groenevelt soil water retention model to predict the hydraulic conductivity, Australian
1072 J. Soil Res., 48, 447-458, 2010.

- 1073 [27] Groenevelt, P. H. and Grant, C. D.: A new model for the soil-water retention curve
1074 that solves the problem of residual water contents, *European J. Soil Sci.*, 55, 479-485,
1075 2004.
- 1076 [28] Gupta, H. V. and Nearing, G. S.: Debates—The future of hydrological sciences: A
1077 (common) path forward? Using models and data to learn: A systems theoretic per-
1078 spective on the future of hydrological science, *Water Resour. Res.*, 50, 5351-5359,
1079 doi:10.1002/2013WR015096, 2014.
- 1080 [29] Harvey, A. H. and Friend, D. G.: Physical properties of water, in *Aqueous systems*
1081 at elevated temperatures and pressures: physical chemistry of water, steam and hy-
1082 drothermal solutions, edited by D. A. Palmer, R. Fernández-Prini and A. H. Harvey,
1083 Elsevier, Amsterdam, The Netherlands, 1-27, 2004.
- 1084 [30] Hellmann, R., Bich, E., Vogel, E., Dickinson, A. S., and Vesovic, V.: Calculation of
1085 the transport and relaxation properties of dilute water vapor, *J. Chem. Phys.*, 131,
1086 014303; doi:10.1063/1.3158830, 2009.
- 1087 [31] Huber, M. L., Perkins, R. A., Laeseche, A., Friend, D. G., Sengers, J. V., Assael, M. J.,
1088 Metaxa, I. N., Vogel, E., Mareš, R., and Miyagawa, K.: New international formulation
1089 for the viscosity of H₂O, *J. Phys. Chem. Ref. Data*, 38, 101-125, 2009.
- 1090 [32] Huber, M. L., Perkins, R. A., Friend, D. G., Sengers, J. V., Assael, M. J., Metaxa, I.
1091 N., Miyagawa, K., Hellmann, R., and Vogel E.: New international formulation for the
1092 thermal conductivity of H₂O, *J. Phys. Chem. Ref. Data*, 41, 033102,
1093 <http://dx.doi.org/10.1063/1.4738955>, 2012.
- 1094 [33] IAPWS [The International Association for the Properties of Water and Steam]: Re-
1095 vised release on the IAPWS industrial formulation 1997 for the thermodynamic prop-

- 1096 erties of water and steam, available at <http://www.iapws.org>, (last access: May 24,
1097 2013), 2007.
- 1098 [34] Jacobs, A. F., and Verhoef, A.: Soil evaporation from sparse natural vegetation esti-
1099 mated from Sherwood numbers, *J. Hydrol.*, 188-189, 443-452, 1997.
- 1100 [35] Jaynes, D. B., and Rogowski, A. S.: Applicability of Ficks law to gas diffusion, *Soil*
1101 *Sci. Soc. Amer. J.*, 47, 425-430, 1983.
- 1102 [36] Jones, H. G.: *Plant and Microclimate*, 3rd Edition, Cambridge University Press, Cam-
1103 bridge, UK, 2014.
- 1104 [37] Jovanović, J. D., Kneženić-Stevanović, A. B., and Grozdanić, D. K.: An empirical
1105 equation for temperature and pressure dependence of liquid heat capacity, *J. Taiwan*
1106 *Inst. Chem. Eng.*, 40, 105-109, 2009.
- 1107 [38] Kadoya, K., Matsunaga, N., and Nagashima, A.: Viscosity and thermal conductivity
1108 of dry air in the gaseous phase, *J. Phys. Chem. Ref. Data*, 14, 947-970, 1985.
- 1109 [39] Kapoor, A., Yang, R. T., and Wong, C.: Surface diffusion, *Catalysis Reviews – Science*
1110 *and Engineering*, 31, 129-214, 1989.
- 1111 [40] Ki, H., Mohanty, P. S., and Mazumder, J.: A numerical method for multiphase in-
1112 compressible thermal flows with solid-liquid and liquid-vapor phase transformations,
1113 *Numerical Heat Transfer, Part B: Fundamentals*, 48, 125-145, 2005.
- 1114 [41] Kon, M., Kobayashi, K. and Watanabe, M.: Method of determining kinetic bound-
1115 ary conditions in net evaporation/condensation, *Physics of Fluids (1994-present)*, 26,
1116 072003, doi:10.1063/1.4890523, 2014.

- 1117 [42] Kozłowski, T.: Modulated Differential Scanning Calorimetry (MDSC) studies on low-
1118 temperature freezing of water adsorbed on clays, apparent specific heat of soil water
1119 and specific heat of dry soil, *Cold Regions Sci. Tech.*, 78, 89-96, 2012.
- 1120 [43] Leij, F. J., Schaap, M. G., and Arya, L. M.: Indirect Methods, in *Methods of Soil*
1121 *Analysis Part 4: Physical Methods*, co-edited by J. H. Dane and G. C. Topp, Soil
1122 Science Society of America Inc., Madison, WI, USA, 1009-1045, 2002.
- 1123 [44] Lynch, D. R.: *Numerical partial differential equations for environmental scientists and*
1124 *engineers*, Springer, New York, NY, 2005.
- 1125 [45] Marrero, T. R. and Mason, E. A.: Gaseous diffusion coefficients, *J. Phys. Chem. Ref.*
1126 *Data*, 1, 3-118, 1972.
- 1127 [46] Massman, W. J.: Modeling soil heating and moisture transport under extreme condi-
1128 tions: Forest fires and slash pile burns, *Water Resour. Res.*, 48, W10548,
1129 doi:10.1029/2011WR011710, 2012.
- 1130 [47] Medveď, I. and Černý, R.: Surface diffusion in porous media: A critical review, *Mi-*
1131 *croporous and Mesoporous Materials*, 142, 405-422, 2011.
- 1132 [48] Miles, R. E. H., Reid, J. P., and R  pinen, I.: Comparison of approaches for measuring
1133 the mass accommodation coefficient for the condensation of water and sensitivities to
1134 uncertainties in thermophysical properties, *J. Phys. Chem. A*, 116, 10810-10825, 2012.
- 1135 [49] Milly, P. C. D.: Moisture and heat-transport in hysteretic, inhomogeneous porous
1136 media: A matric head-based formulation and a numerical model, *Water Resour. Res.*,
1137 18, 489-498, 1982.

- 1138 [50] Moldrup, P. T., Olesen, D. E., Roslton, D. E., and Yamaguchi, T.: Modeling diffusion
1139 and reactions in soils: VII. Predicting gas and ion diffusivity in undisturbed and sieved
1140 soils, *Soil Sci.*, 162, 632-640, 1997.
- 1141 [51] Novak, M. D.: Dynamics of the near-surface evaporation zone and corresponding effects
1142 on the surface energy balance of a drying soil, *Ag. For. Meteorol.*, 150, 1358-1365, 2010.
- 1143 [52] Novak, M. D.: Comment on “Evaporation from soils under thermal boundary
1144 conditions: Experimental and modeling investigation to compare equilibrium- and
1145 nonequilibrium-based approaches” by Kathleen M. Smits, Abdullah Cihan, Toshi-
1146 hiro Sakaki, and Tissa H. Illangasekare, *Water Resources Research*, 48, W05549,
1147 doi:10.1029/2011WR011393, 2012.
- 1148 [53] Ouedraogo, F., Cherblanc, F., Naon, B., and Bénét, J.-C.: Water transfer in soil at
1149 low water content. Is the local equilibrium assumption still appropriate?, *J. Hydrology*
1150 492, 117-127, 2013.
- 1151 [54] Pakala, V. K. C. and Plumb, O. A.: High intensity drying in porous materials, *J.*
1152 *Thermal Sci. Eng. Appls.*, 4, 021010, doi:/10.1115/1.4006275, 2012.
- 1153 [55] Philip, J. R. and de Vries, D. A.: Moisture movement in porous materials under
1154 temperature gradients, *EOS Trans. AGU*, 38, 222-232, 1957.
- 1155 [56] Sato, H.: An equation of state for the thermodynamic properties of water in the liquid
1156 phase including the metastable state, in *Properties of Water and Steam Proceedings*
1157 *of the 11th International Conference*, edited by M. Píchal and O. Šifner, Hemisphere
1158 Publishing Company, New York, NY, USA, 48-55, 1990.
- 1159 [57] Shiozawa, S., and Campbell, G. S.: On the calculation of mean particle diameter and
1160 standard deviation from sand, silt, and clay fractions, *Soil Science*, 152, 427-431, 1991.

- 1161 [58] Skopp, J.: Oxygen uptake and transport in soils: analysis of the air-water interfacial
1162 area, *Soil Sci. Soc. Amer. J.*, 49, 1327-1331, 1985.
- 1163 [59] Smits, K. M., Cihan, A., Sakaki, T., and Illangasekare, T. H.: Evaporation from
1164 soils under thermal boundary conditions: Experimental and modeling investigation to
1165 compare equilibrium- and nonequilibrium-based approaches, *Water Resour. Res.*, 47,
1166 W05540, doi:10.1029/2010WR009533, 2011.
- 1167 [60] Smits, K. M., Ngo, V. V., Cihan, A., Sakaki, T., and Illangasekare T. H.:
1168 An evaluation of models of bare soil evaporation formulated with different land
1169 surface boundary conditions and assumptions, *Water Resour. Res.*, 48, W12526,
1170 doi:10.1029/2012WR012113, 2012.
- 1171 [61] Solsvik, J., and Jakobsen, H. A.: A Survey of multicomponent mass diffusion flux
1172 closures for porous pellets: Mass and molar forms, *Transp. Porous Med.*, 93, 99-126,
1173 2012, doi:10.1007/s11242-012-9946-7.
- 1174 [62] Somayajulu, G. R.: New equations for enthalpy of vaporization from the triple point
1175 to the critical point, *Int. J. Thermophysics*, 9, 567-575, 1988.
- 1176 [63] Thomas, J. C.: Numerical partial differential equations: finite difference methods,
1177 Springer, New York, NY, USA, 1985.
- 1178 [64] Tsilingiris, P. T.: Thermophysical transport properties of humid air at temperature
1179 range between 0 and 100 C, *Energy Conservation and Management*, 49, 1098-1110,
1180 2008.
- 1181 [65] Tsuruta, T. and Nagayama, G.: Molecular dynamics studies on the condensation
1182 coefficient of water, *J. Phys. Chem. B*, 108, 1736-1743, 2004.

- 1183 [66] Udell, K. S.: Heat transfer in porous media heated from above with evaporation,
1184 condensation, and capillary effects, *J. Heat Trans.*, 105, 485-492, 1983.
- 1185 [67] Van Genuchten, M. Th. and Nielsen, D. R.: On describing and predicting the hydraulic
1186 properties of unsaturated soils, *Annales Geophysicae*, 3, 615-628, 1985.
- 1187 [68] Vargaftik, N. B., Volkov, B. N. and Voljak, L. D.: International tables of the surface
1188 tension of water, *J. Phys. Chem. Ref. Data*, 12, 817-820, 1983.
- 1189 [69] Wagner, W. and Pruess, A.: The IAPWS formulation 1995 for the thermodynamic
1190 properties of ordinary water substance for general and scientific use, *J. Phys. Chem.*
1191 *Ref. Data*, 31, 387-535, 2002.
- 1192 [70] Whitaker, S.: Simultaneous heat, mass and momentum transfer in porous media: a
1193 theory of drying, *Adv. Heat Trans.*, 13, 119-203, 1977.
- 1194 [71] Whitaker, S. and Chou, W. T.-H.: Drying granular porous media – Theory and ex-
1195 periment, *Drying Technol.*, 1, 3-33, 1983-1984.
- 1196 [72] Yaws, C.: *Handbook of Transport Property Data*, Gulf Publishing Company, Houston,
1197 TX, USA, 1985.
- 1198 [73] Yoshida, K., Matubayasi, N., and Nakahara, M.: Self-diffusion of supercritical water
1199 in extremely low-density region, *J. Chem. Phys.*, 125, 074307; doi:10.1063/1.2333511,
1200 2006.
- 1201 [74] Yoshida, K., Matubayasi, N., and Nakahara, M.: Erratum: Self-diffusion of super-
1202 critical water in extremely low-density region [*J. Chem. Phys.* 125, 074307 (2006)], *J.*
1203 *Chem. Phys.*, 126, 089901; doi:10.1063/1.2372501, 2007.

1204 [75] Zhang, Z. F.: Soil water retention and relative permeability for conditions from oven-
1205 dry to full saturation, Vadose Zone J., 10, 1299-1308, doi:10.2136/vzj2011.0019, 2011.

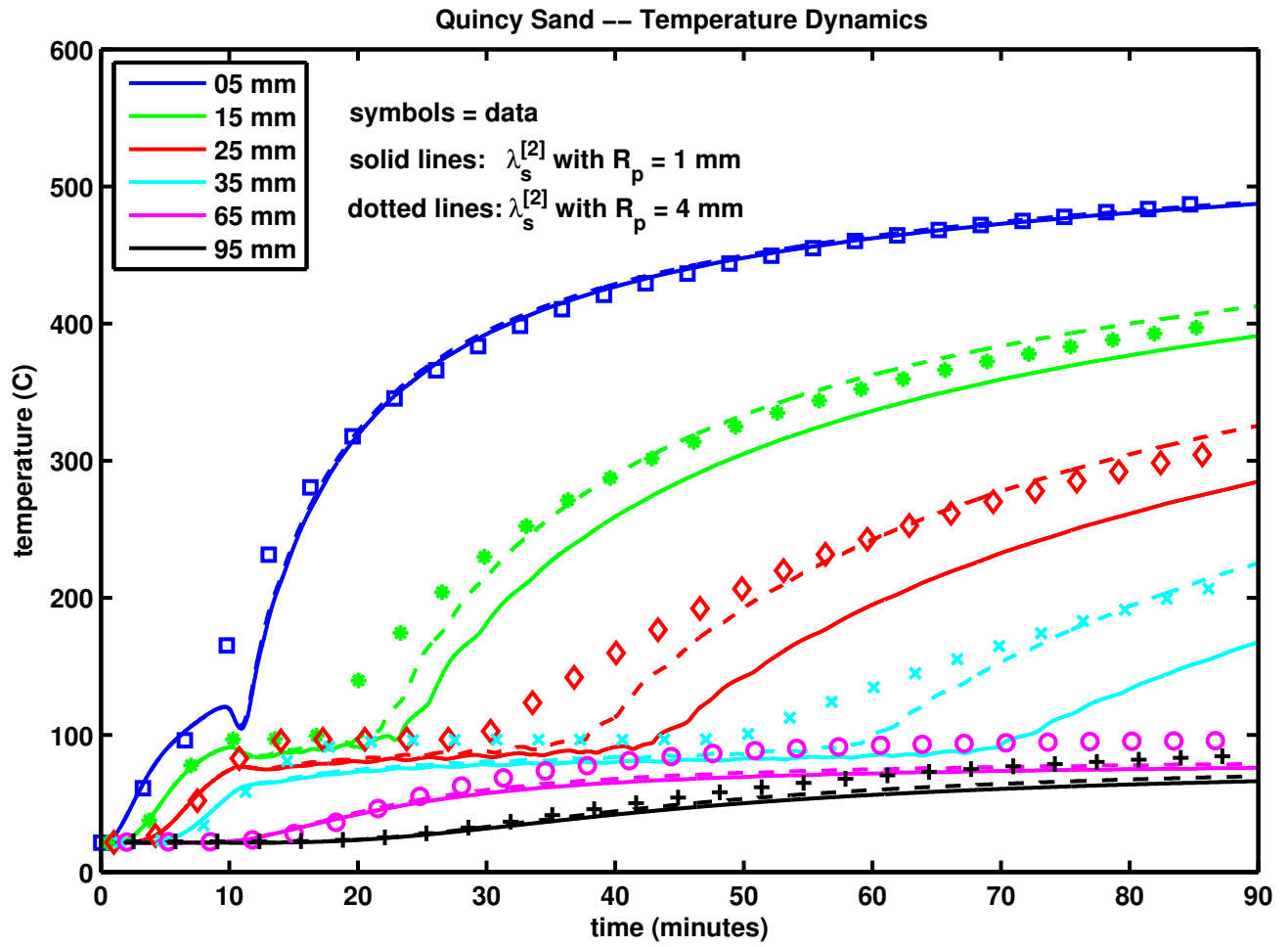


Figure 1:

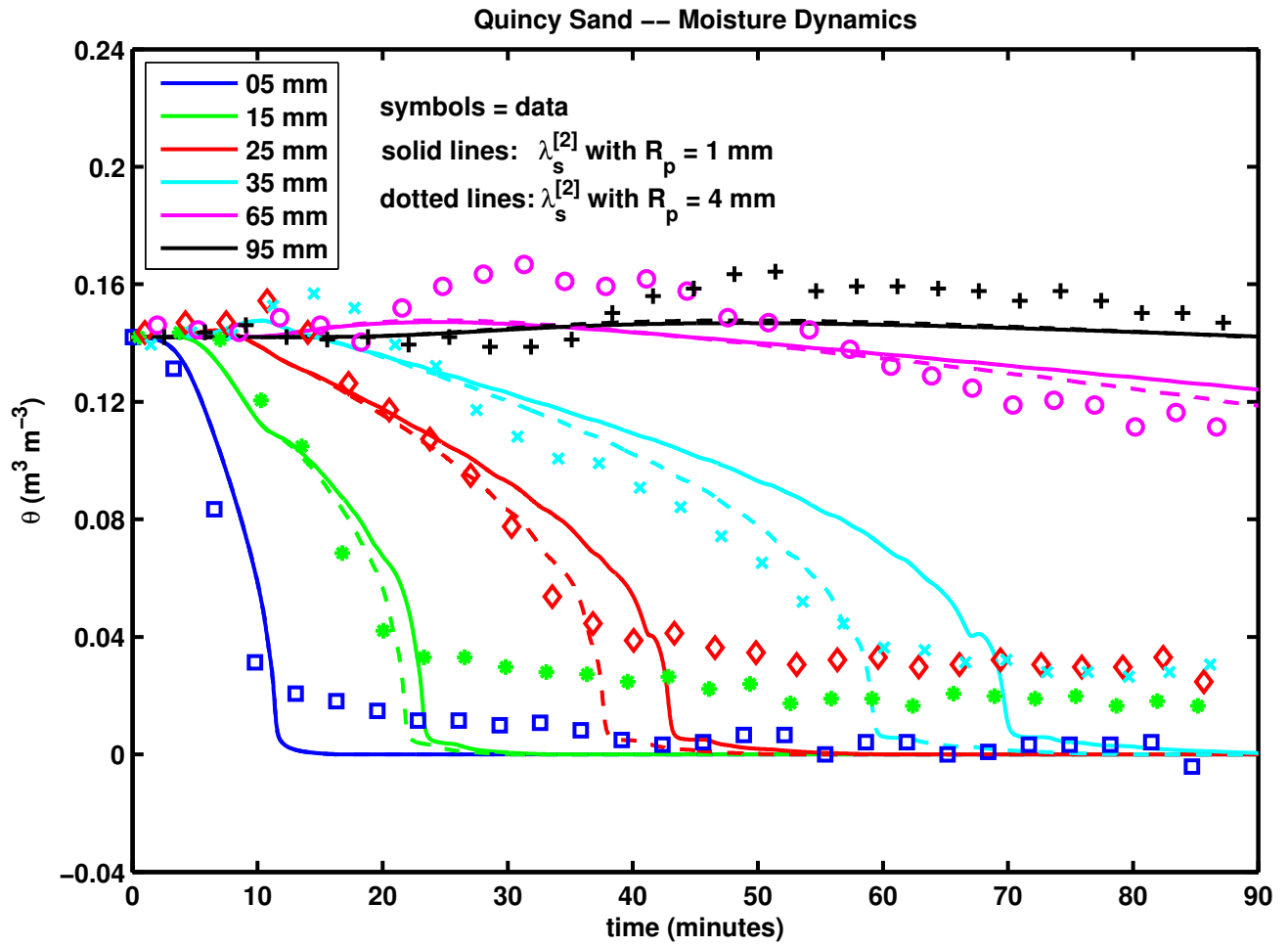


Figure 2:

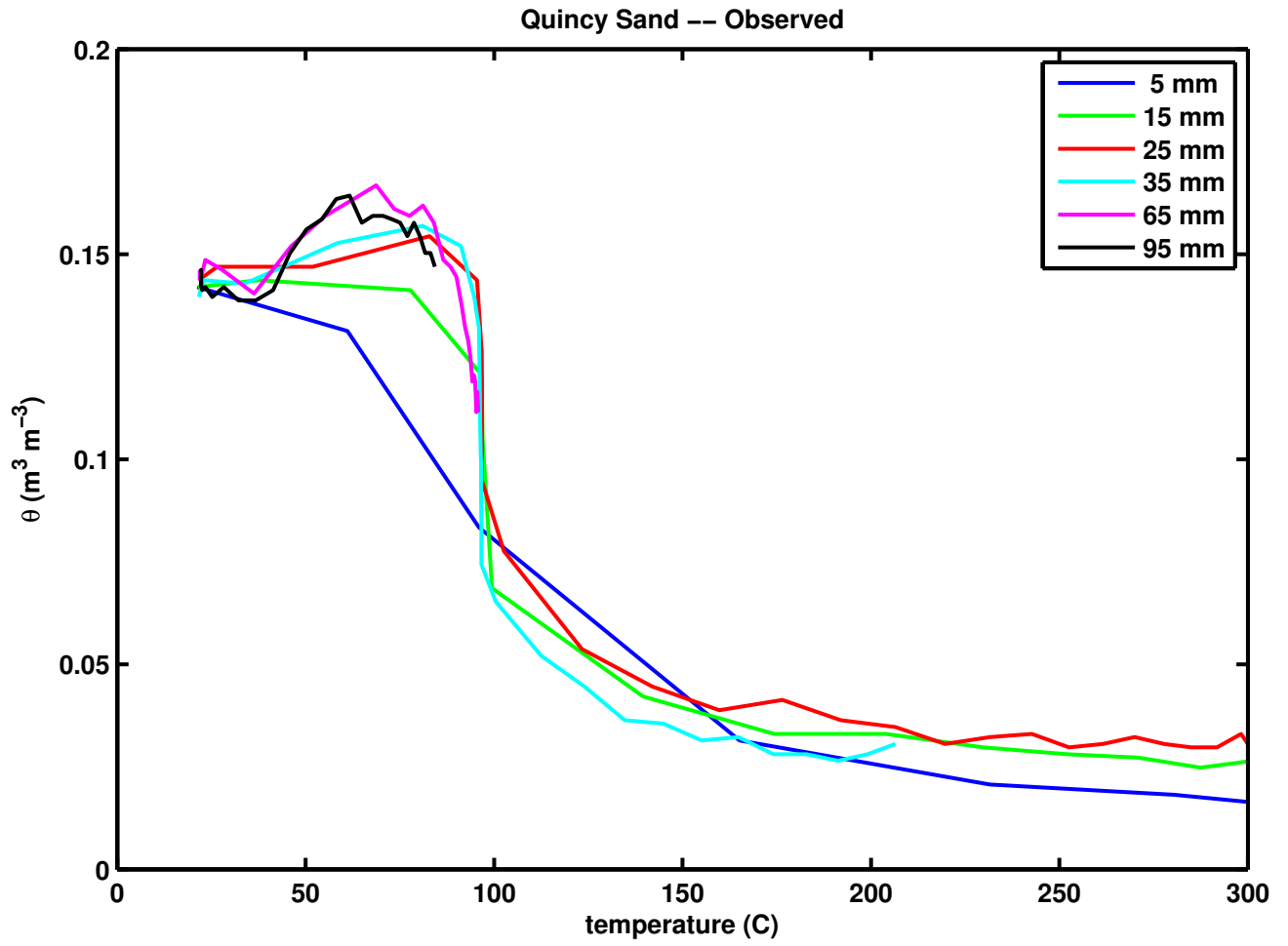


Figure 3:

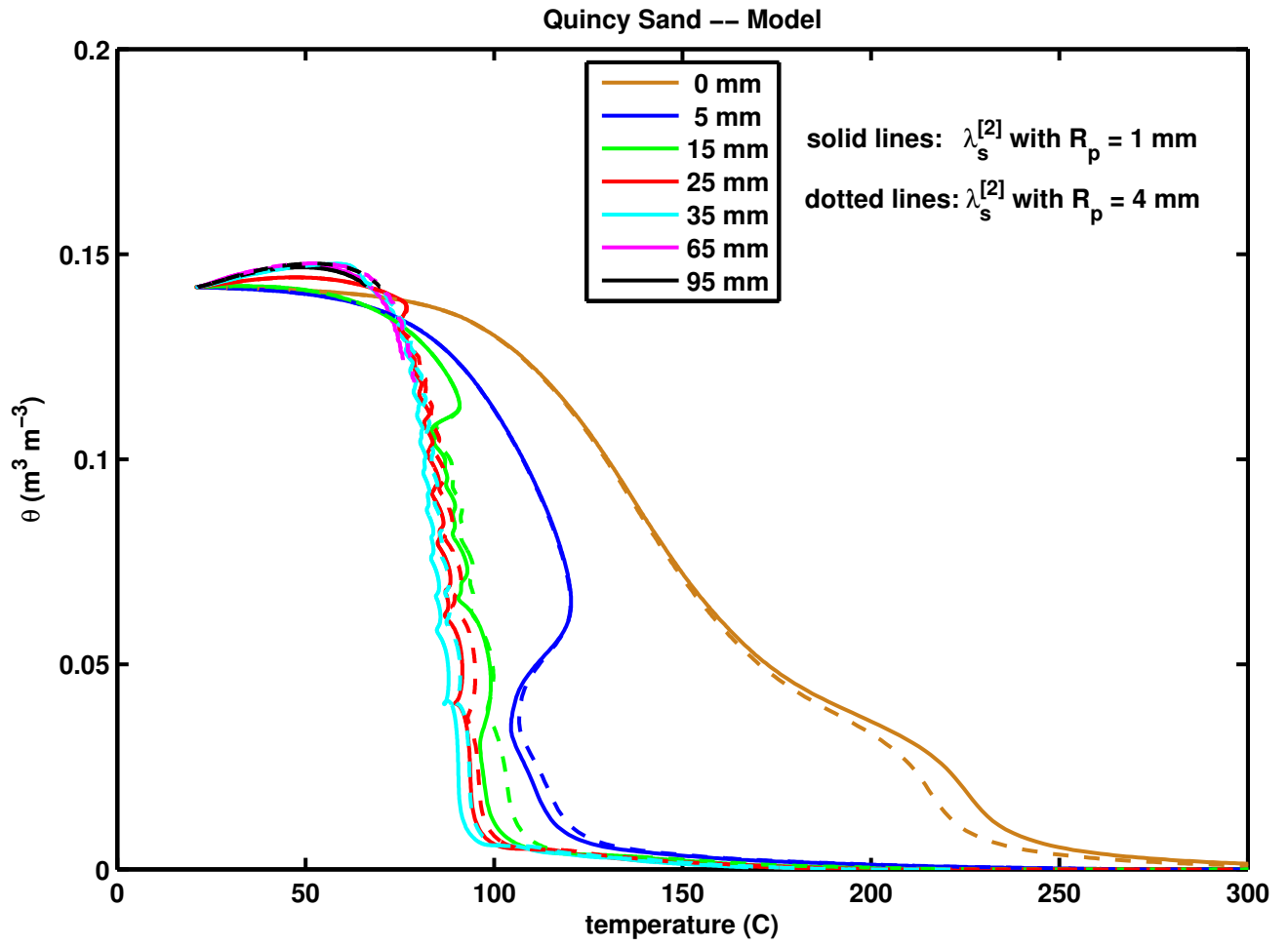


Figure 4:

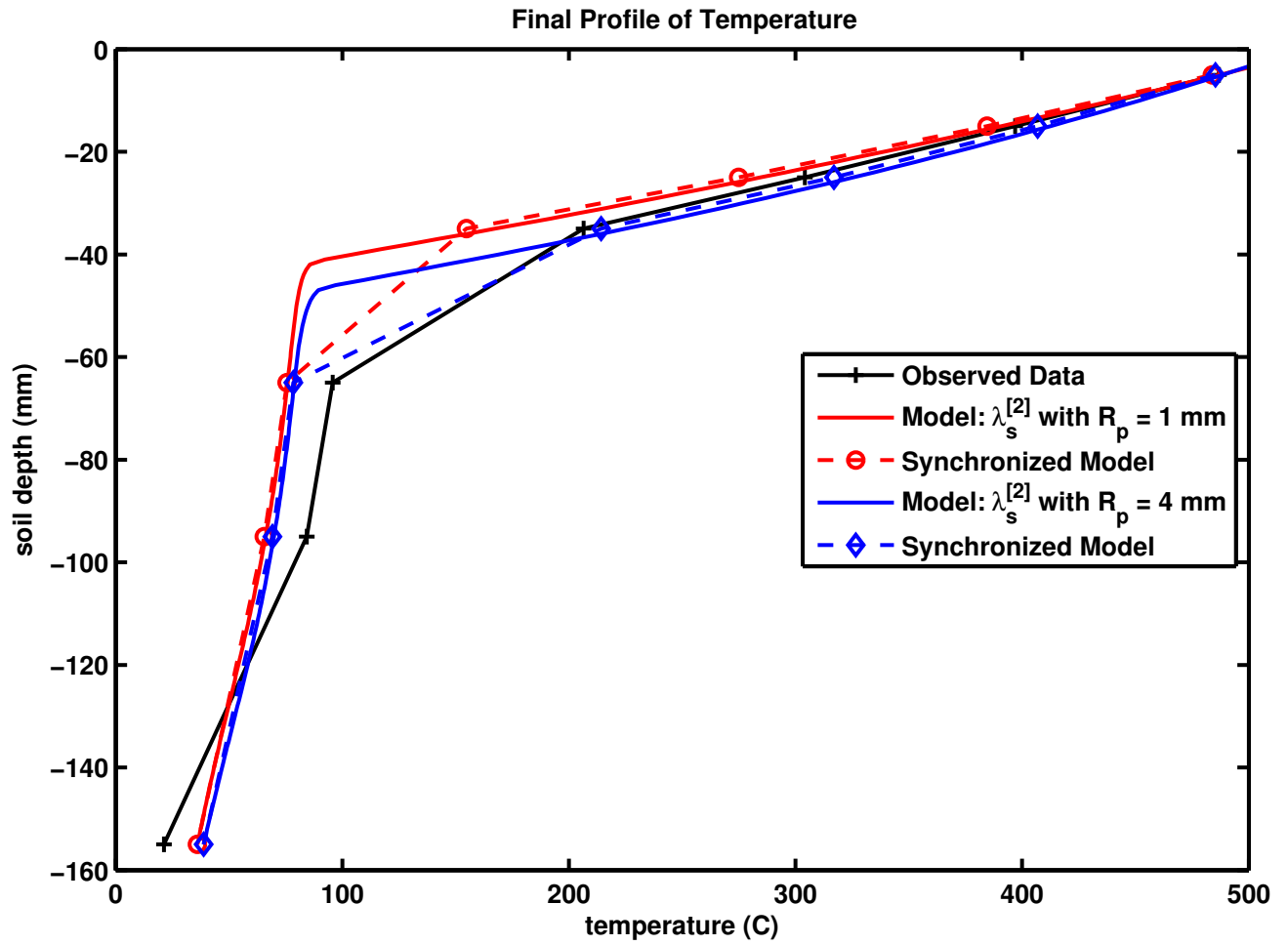


Figure 5:

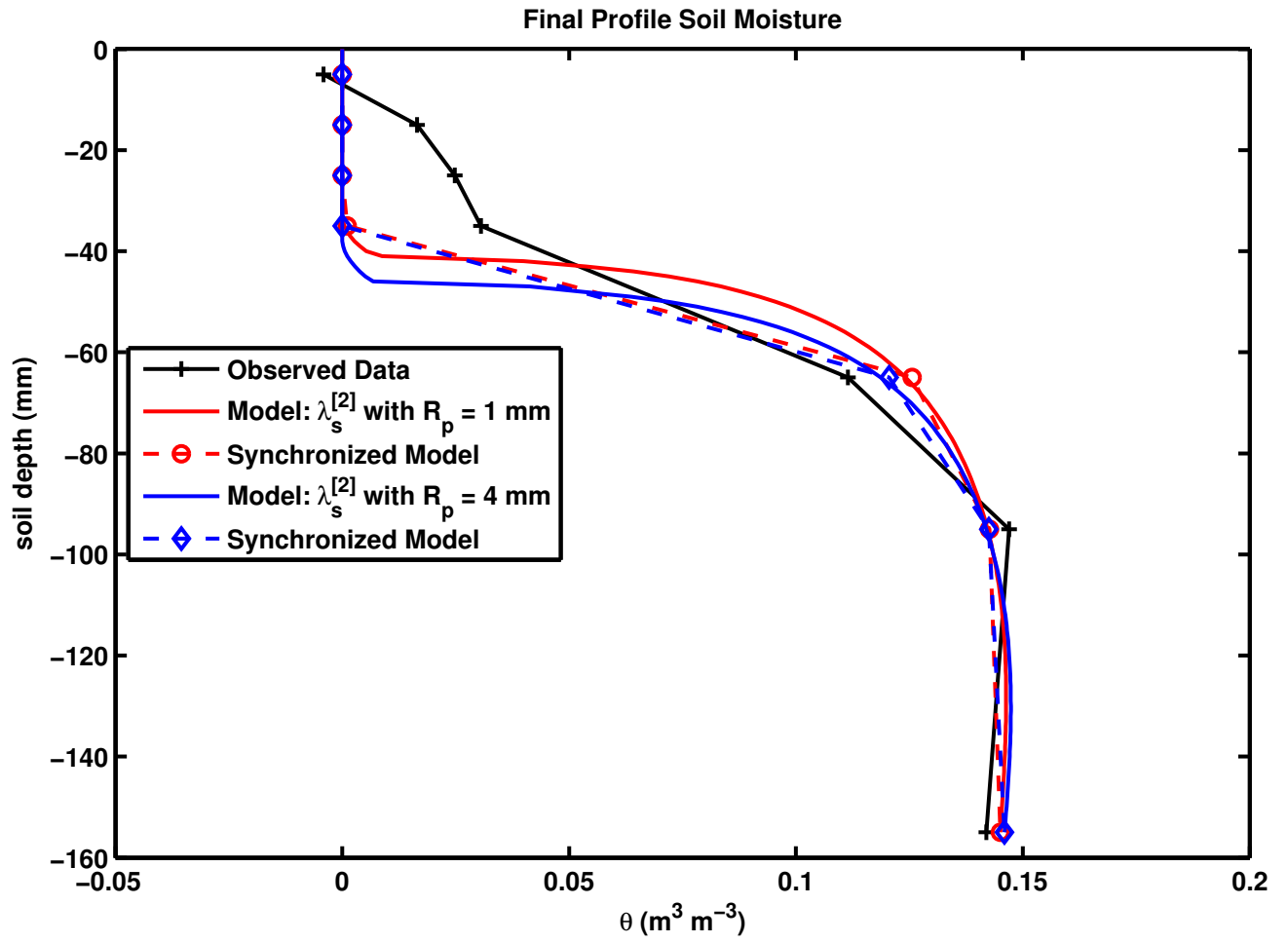


Figure 6:

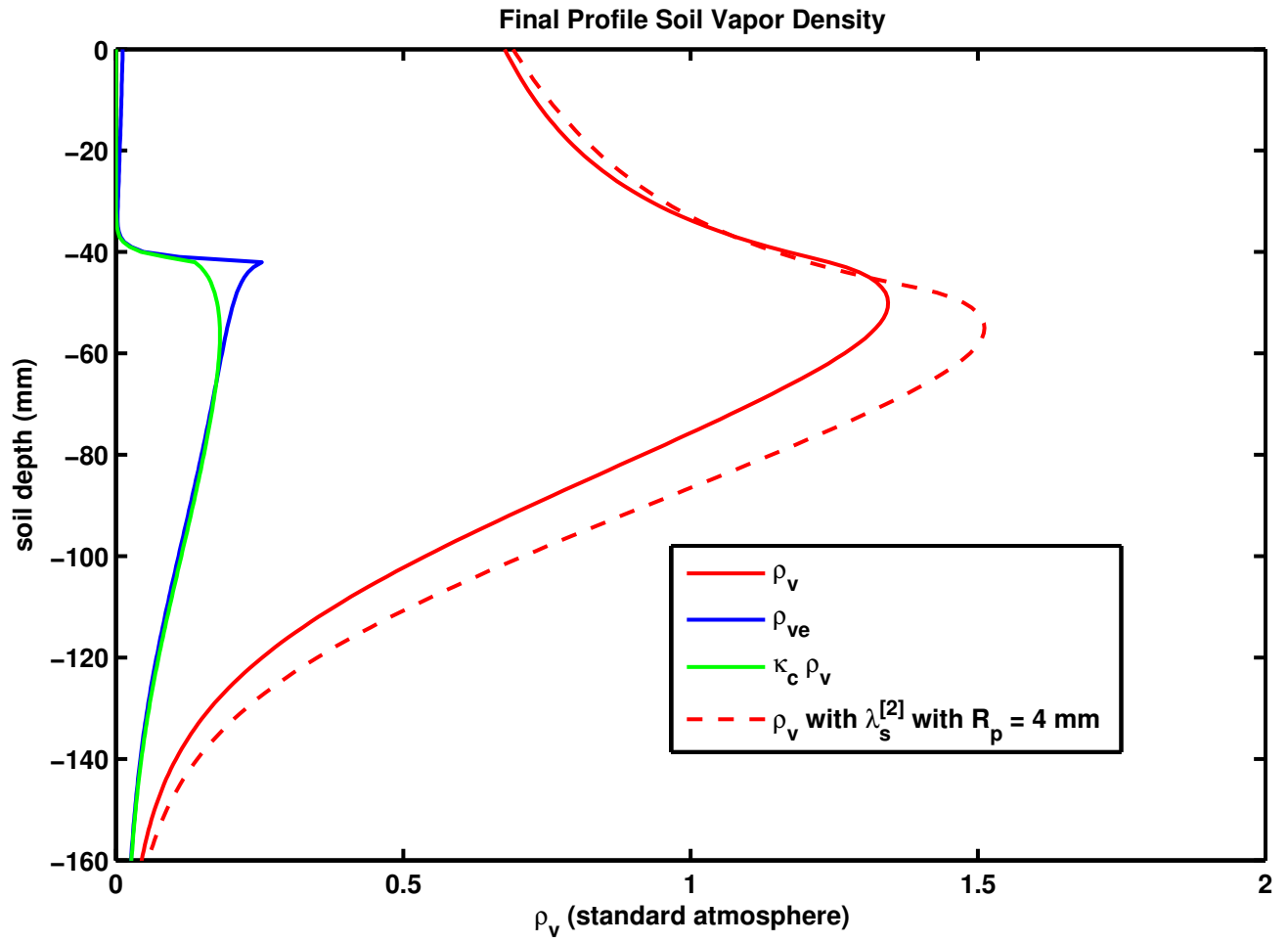


Figure 7:

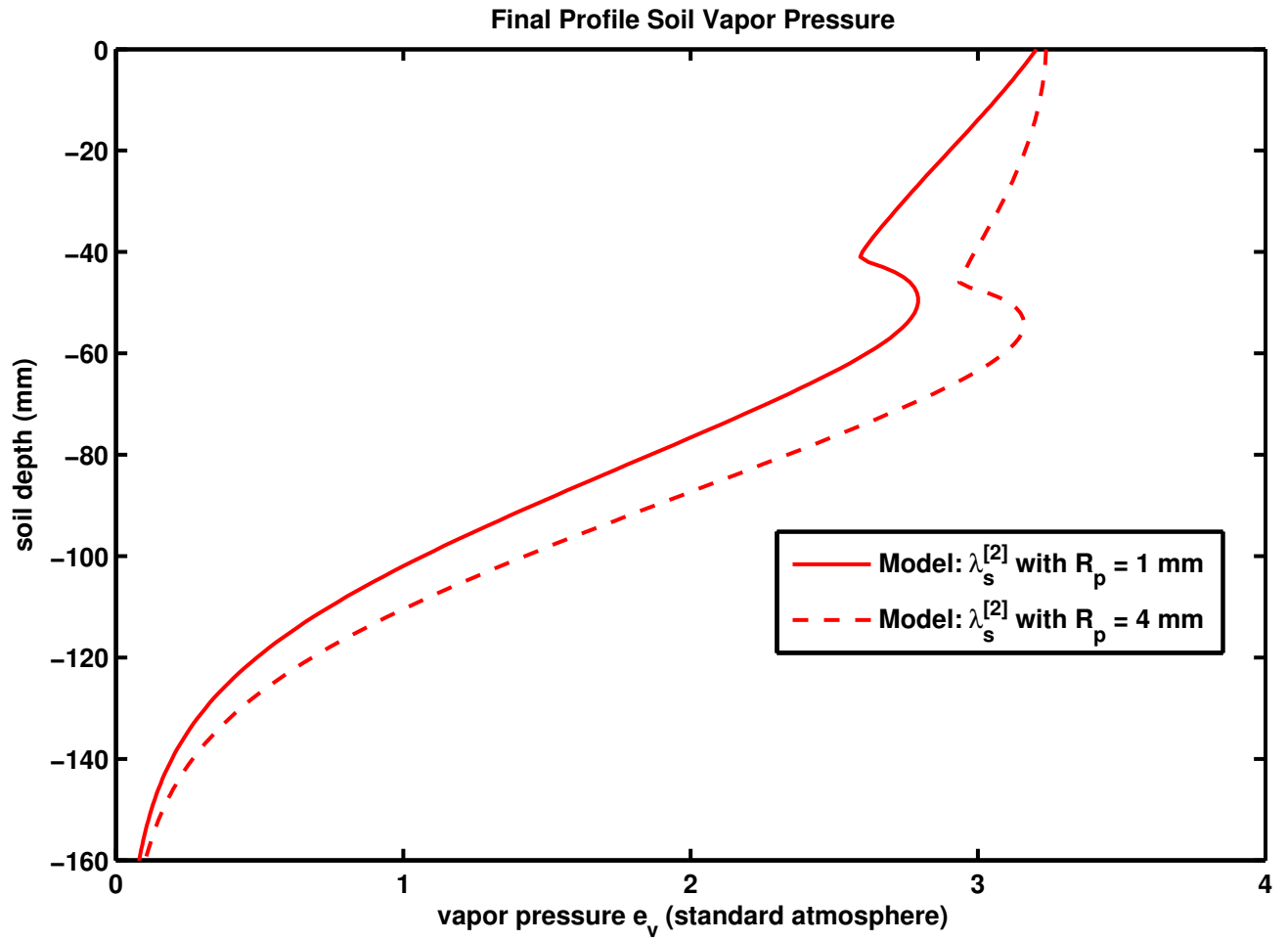


Figure 8:

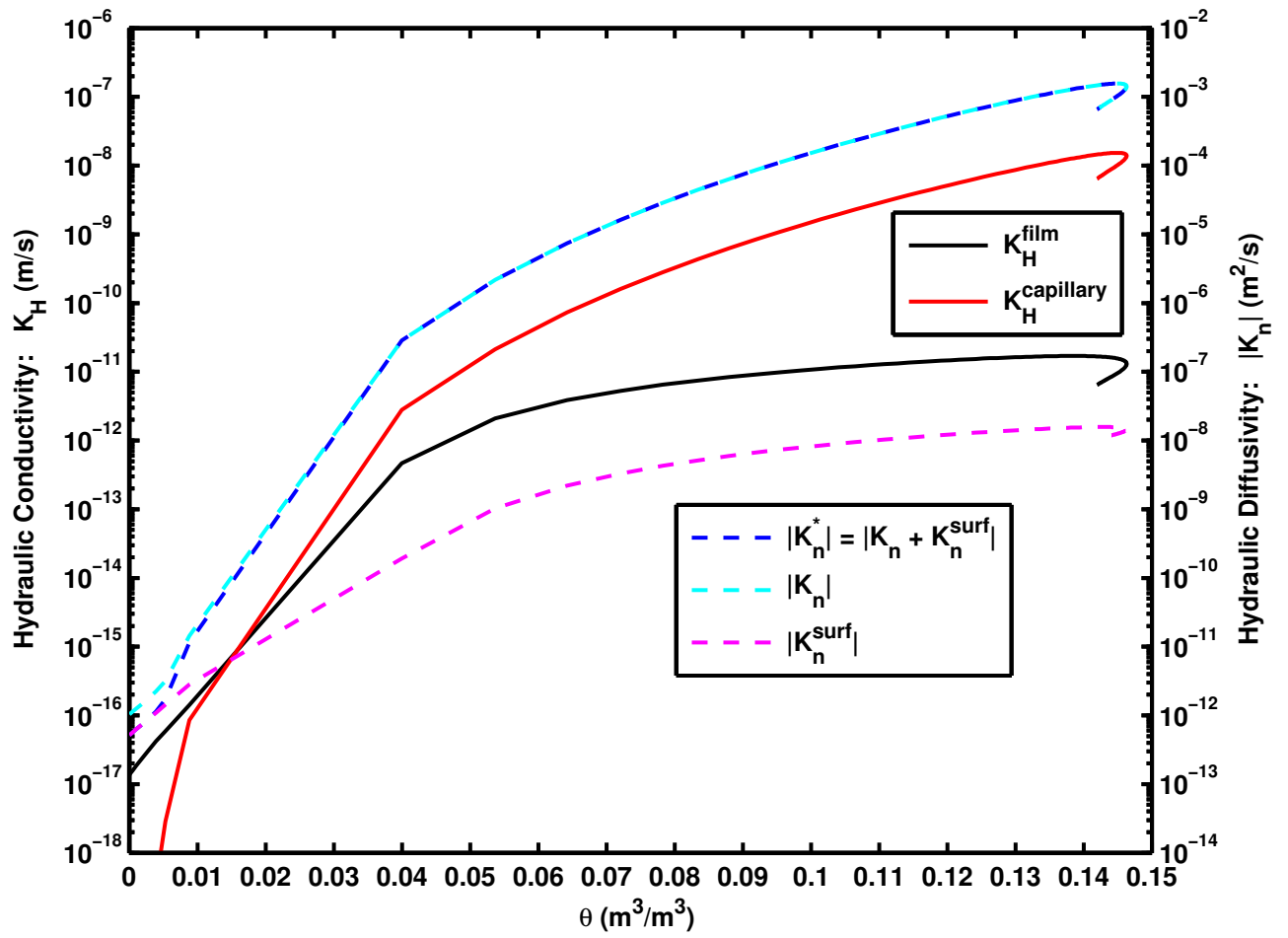


Figure 9:

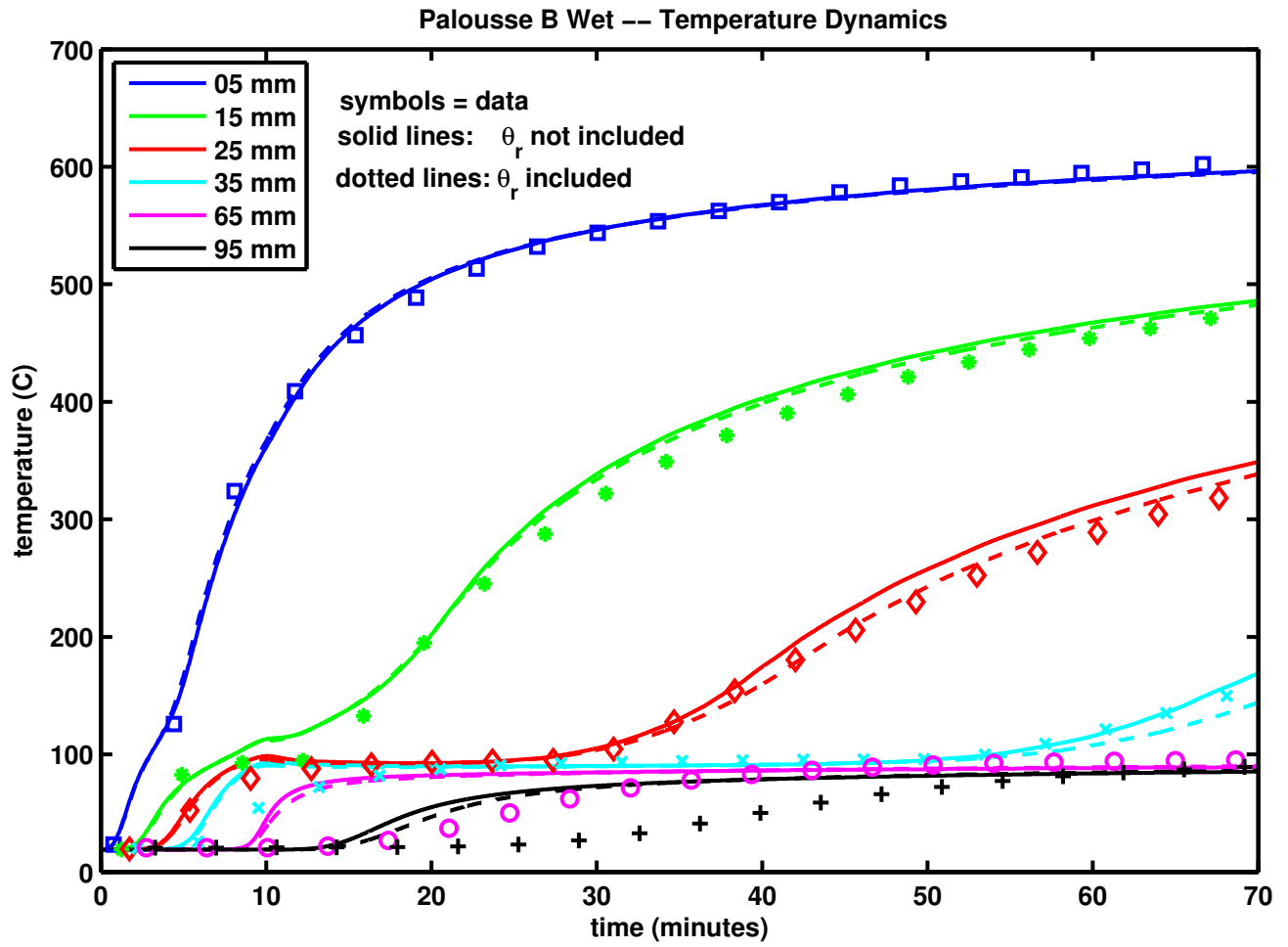


Figure 10:

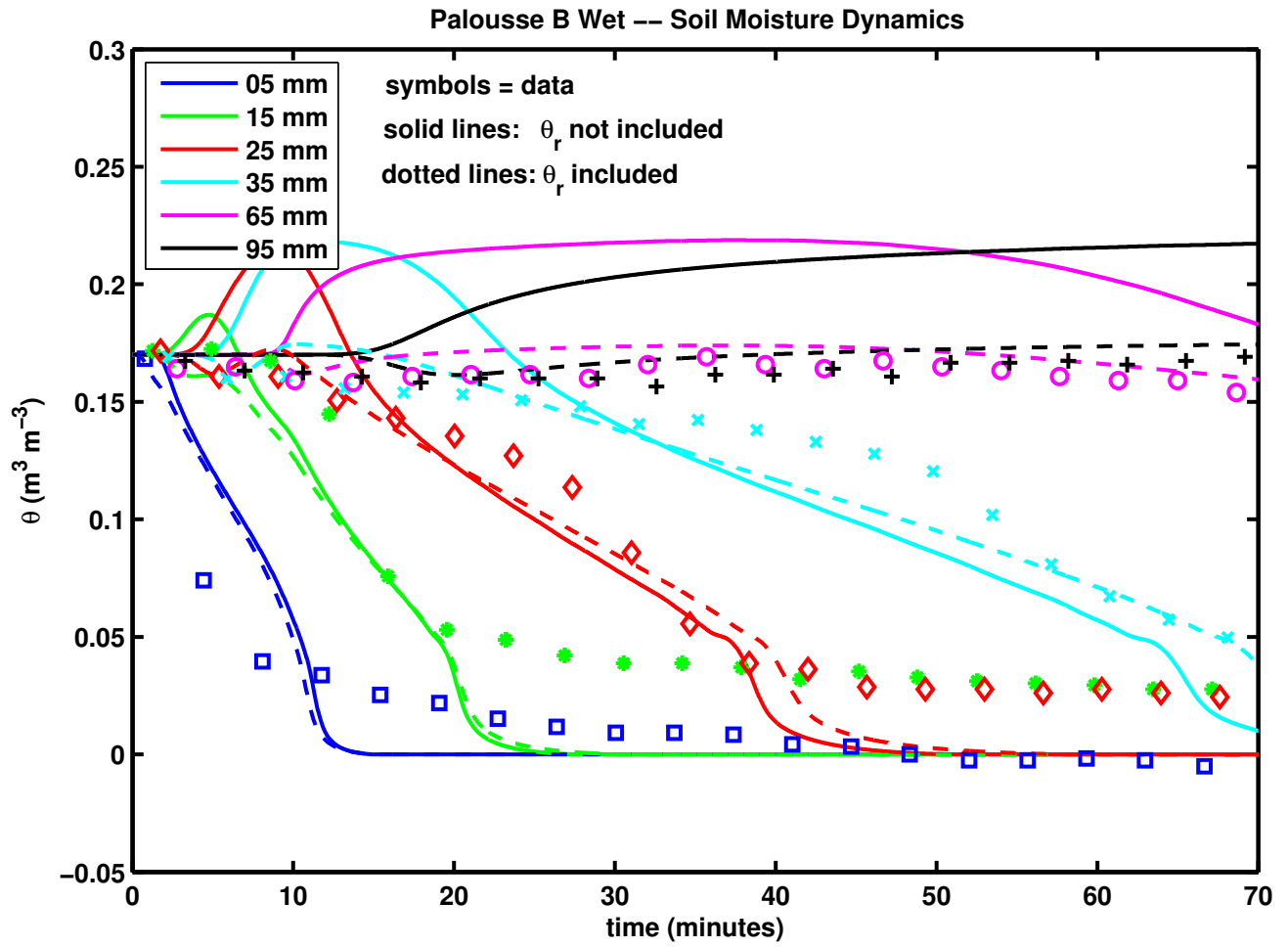


Figure 11:

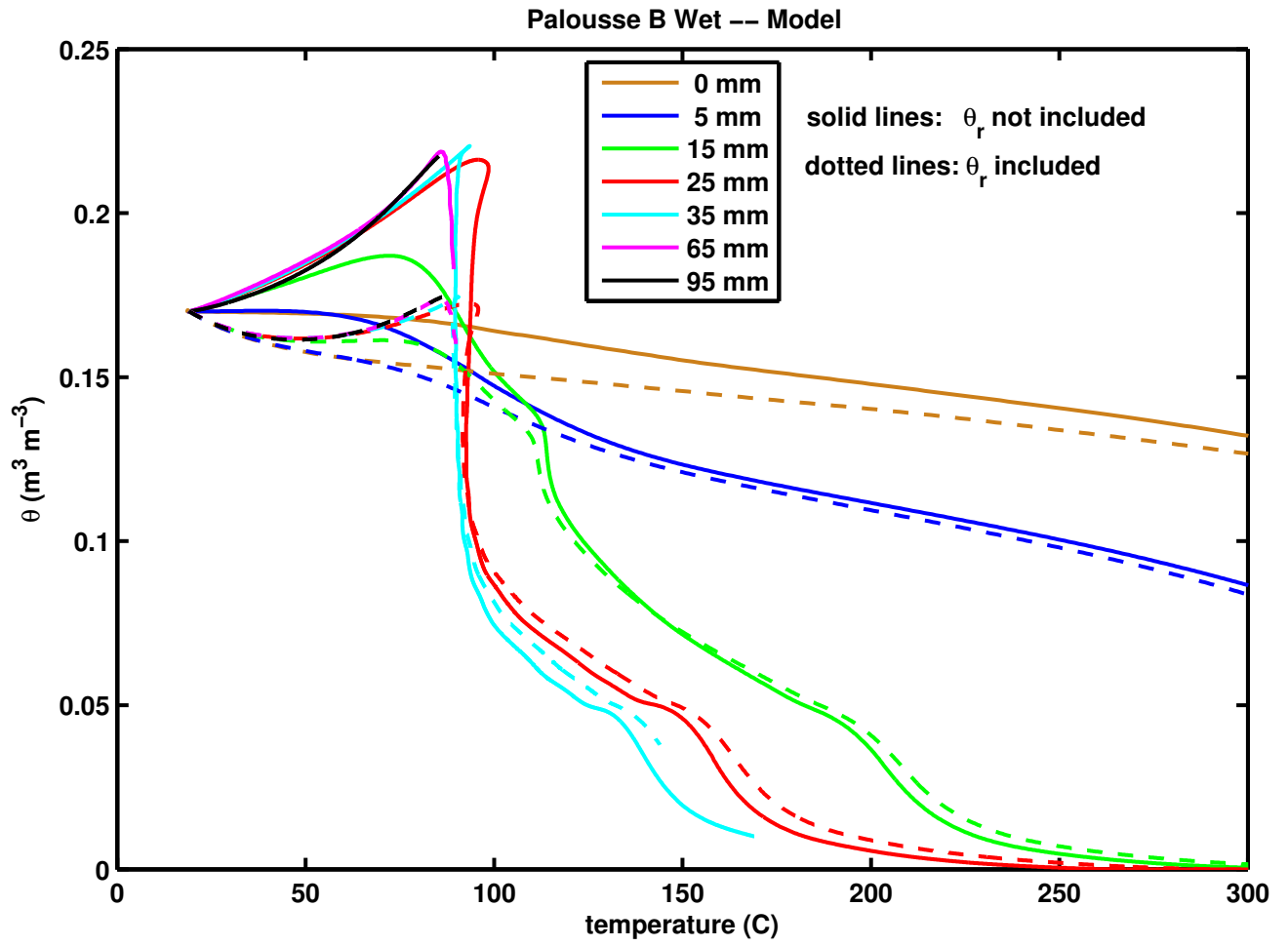


Figure 12:

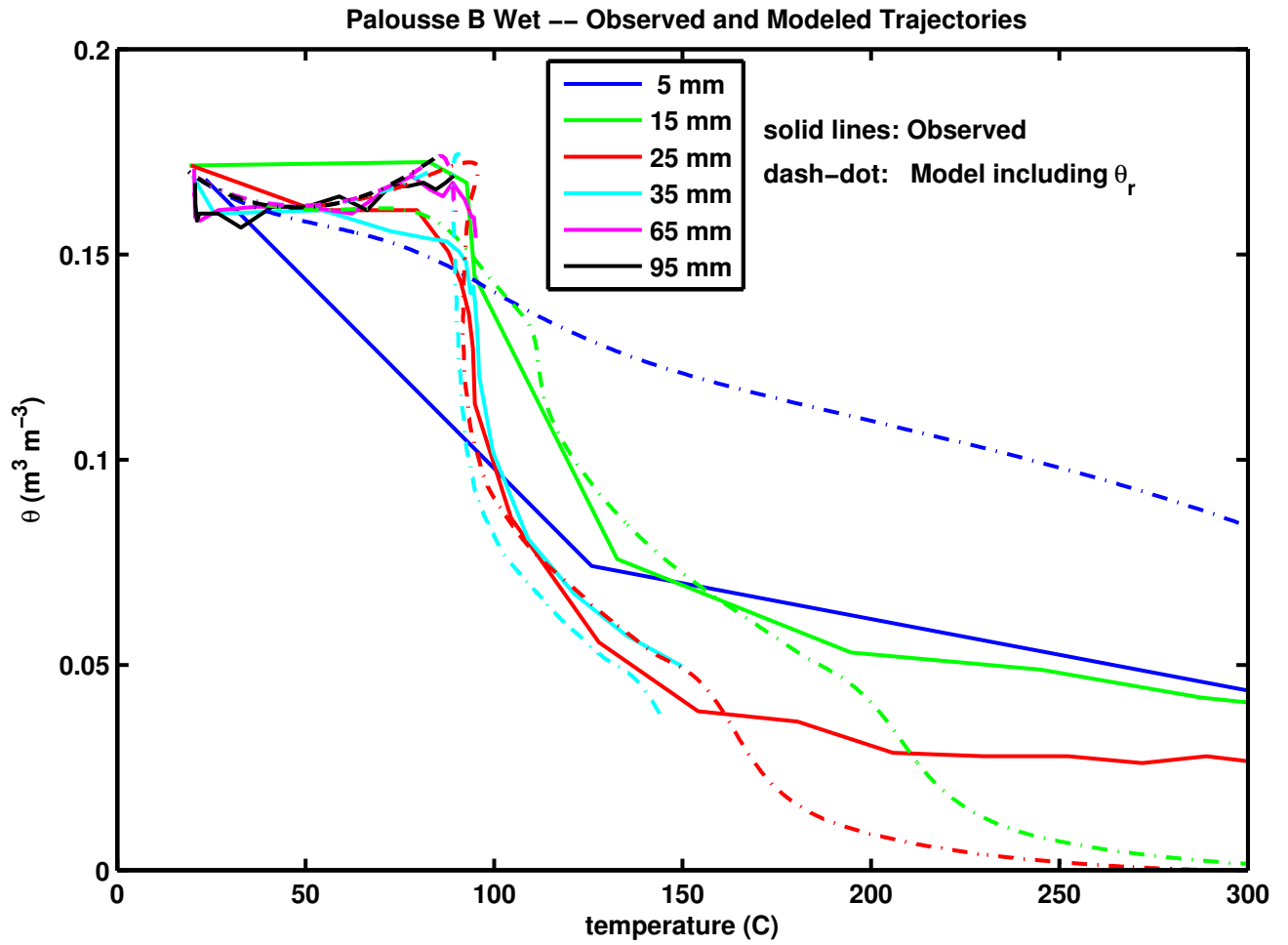


Figure 13:

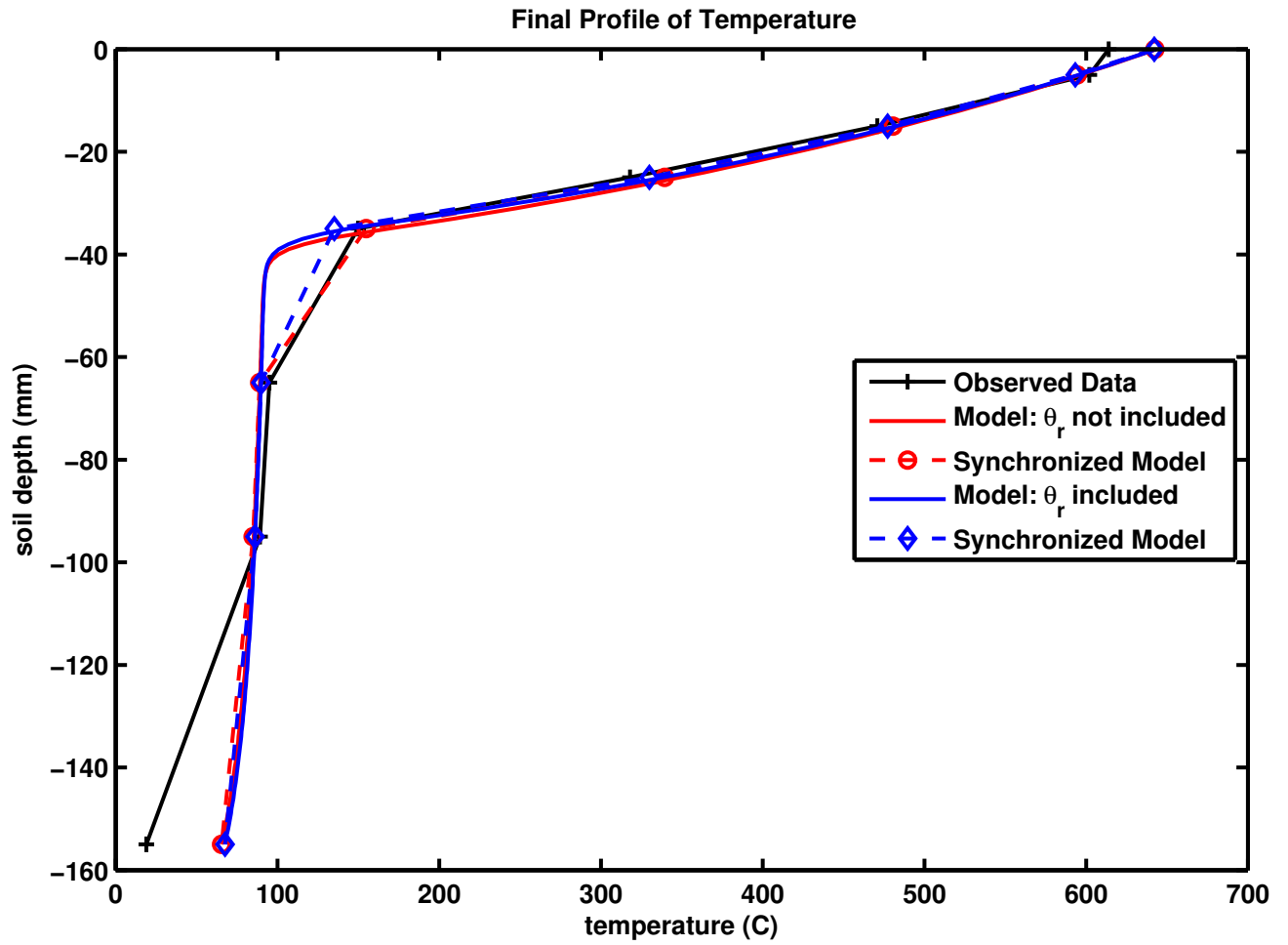


Figure 14:

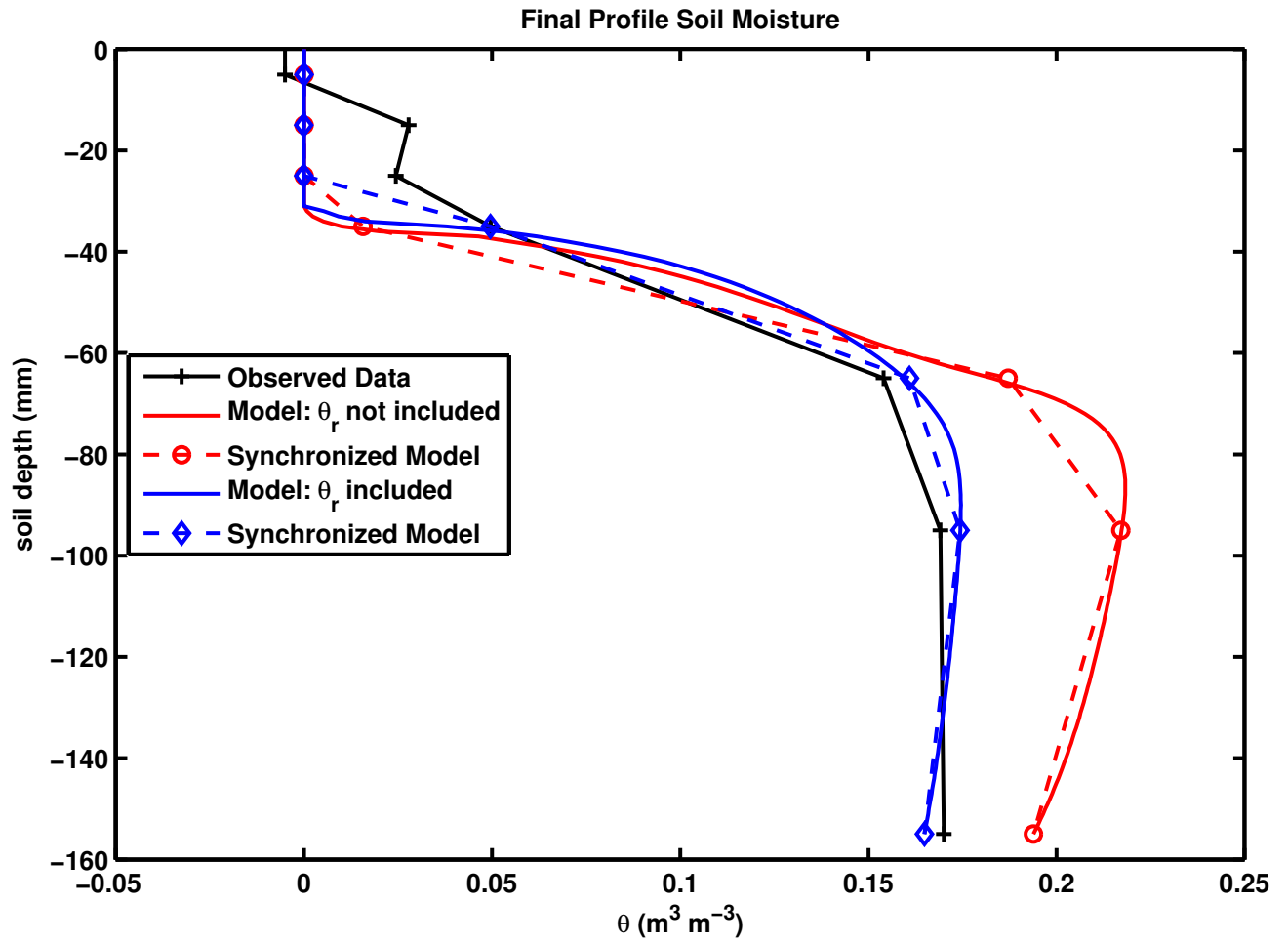


Figure 15:

1206 **Figure Captions**

1207 **Figure 1.** Comparison of measured (symbols) and modeled (lines) soil temperatures during
1208 the Quincy Sand heating experiment. Neither simulation includes a dynamic residual soil
1209 moisture term, θ_r . The solid lines are for a model simulation with $R_p = 1$ mm; the dotted
1210 lines corresponds to a simulation for $R_p = 4$ mm. Note as R_p increases the infrared portion
1211 of the soil thermal conductivity, $\lambda_s^{[2]}$, also increases, in accordance with Equation (14). To
1212 compare with the equilibrium model see Figure 2 of *Massman 2012*.

1213 **Figure 2.** Comparison of measured (symbols) and modeled (lines) soil moisture contents
1214 during the Quincy Sand heating experiment. Neither simulation includes a dynamic residual
1215 soil moisture term, θ_r . The solid lines are for a model simulation with $R_p = 1$ mm; the
1216 dotted lines correspond to a simulation with $R_p = 4$ mm. To compare with the equilibrium
1217 model see Figure 3 of *Massman 2012*.

1218 **Figure 3.** Measured soil moisture vs measured soil temperatures for the Quincy Sand
1219 heating experiment (see previous two figures).

1220 **Figure 4.** Modeled soil moisture contents vs modeled soil temperatures for the Quincy Sand
1221 heating experiment (see Figs. 1 and 2 above). The solid lines are for a model simulation
1222 with $R_p = 1$ mm; the dotted lines correspond to a simulation with $R_p = 4$ mm. This is the
1223 solution space representation of the model's solutions, which are to be compared with the
1224 observations shown in the preceding figure, Fig. 3, as well as with the equilibrium model
1225 results shown in Figure 5 of *Massman 2012* .

1226 **Figure 5.** Comparison of the final modeled and measured temperature profiles at the
1227 completion of the 90-minute Quincy Sand heating experiment. Because the data shown in
1228 the measured profile (black) are not precisely coincident in time, the full model results (solid
1229 red and blue lines) were sub-sampled in synchrony in time (and coincide in space) with the

1230 observations. These time-synchronized model profiles are shown as dashed red and blue
1231 lines. To compare with the equilibrium model see Figure 6 of *Massman* 2012.

1232 **Figure 6.** Comparison of the final modeled and measured moisture profiles at the completion
1233 of the Quincy Sand heating experiment. Because the data shown in the measured profile
1234 (black) are not precisely coincident in time, the full model results (solid red and blue lines)
1235 were sub-sampled in synchrony in time (and coincide in space) with the observations. These
1236 synchronized model profiles are shown as dashed red and blue lines. The observed data
1237 (black) suggest that the total water lost during the 90-minute experiment was 31% of the
1238 initial amount. The (red) model simulation indicated a 31.4% loss and the corresponding
1239 (red) synchronized-model yielded a 33.8% loss. The (blue) model simulation indicated a
1240 34.6% loss and the corresponding (blue) synchronized-model yielded a 34.2% loss. Note
1241 there is very little recondensing soil moisture ahead of the drying front (at about 40-50 mm
1242 depth), in agreement with Figures 2 and 4 above and in contrast with the equilibrium model,
1243 Figure 7 of *Massman* 2012, where there was significant recondensation.

1244 **Figure 7.** Final modeled profiles of vapor density $[\rho_v]$, equilibrium vapor density $[\rho_{ve}]$, and
1245 the condensation coefficient (\mathcal{K}_c) modified vapor density term $[\mathcal{K}_c\rho_v]$ used with the non-
1246 equilibrium model source term, S_v , at the completion of the 90-minute model simulation.
1247 The three solid lines are for a model simulation with $R_p = 1$ mm; the single dotted line
1248 corresponds to a simulation with $R_p = 4$ mm. The maximum vapor density for these two
1249 simulations is between about 1.3 and 1.5 times the density of the standard atmosphere (=
1250 1.292 kg m^{-3}) and is located the near position of the maximum in the vapor source term,
1251 S_v . This figure can be compared with the equilibrium model result: Figure 8 of *Massman*
1252 2012.

1253 **Figure 8.** Final modeled profile of vapor pressure at the end of the 90-minute model

1254 simulation. The solid line is the model simulation with $R_p = 1$ mm and the dotted line
1255 corresponds to the simulation with $R_p = 4$ mm. In both cases the maximum vapor pressure
1256 occurs at the soil surface and/or near the level of the maximum S_v . For these two scenarios
1257 the maximum vapor pressure is about 3.2 times the pressure of one standard atmosphere (= $P_{ST} = 101.325$ kPa).
1258

1259 **Figure 9.** Example of the hydraulic conductivity, K_H , and magnitude of the hydraulic
1260 diffusivity, $|K_n|$, as functions of soil moisture, θ , for the Quincy Sand $R_p = 1$ mm scenario.
1261 K_H corresponds to *Assouline's* [2001] HCF for capillary flow, Equation (17), and *Zhang's*
1262 [2011] model for film flow, Equation (18). Numerically $|K_n|$ is just a rescaling of K_H (see
1263 Section 2.2.5 for further details) and $|K_n^{surf}|$ is derived from the *Gawin's* [1999] model for
1264 $V_{\theta, surf}$ (again see section 2.2.5).

1265 **Figure 10.** Comparison of measured (symbols) and modeled (lines) soil temperature during
1266 the Palousse B Wet heating experiment. The solid lines are for a model simulation that
1267 does not include the dynamic residual soil moisture, θ_r ; the dotted lines correspond to the
1268 simulation that includes θ_r .

1269 **Figure 11.** Comparison of measured (symbols) and modeled (lines) soil moisture content
1270 during the Palousse B Wet heating experiment. The solid lines are for a model simulation
1271 that does not include the dynamic residual soil moisture, θ_r ; the dotted lines correspond to
1272 a simulation that includes θ_r . For this experiment the initial soil moisture, θ_{in} , is 0.17 m^3
1273 m^{-3} .

1274 **Figure 12.** Modeled soil moisture vs modeled soil temperatures for the Palousse B Wet
1275 heating experiment (see Figs. 10 and 11 above). The solid lines are for a model simulation
1276 that does not include the dynamic residual soil moisture, θ_r ; the dotted lines correspond
1277 to a simulation that includes θ_r . This is the solution space representation of the model's

1278 solutions.

1279 **Figure 13.** Observed and modeled soil moisture vs soil temperatures (trajectories) for the
1280 Wet Palouisse B heating experiment. Solid lines are observed data and the dash-dot lines are
1281 from the model that includes the dynamic residual soil moisture, θ_r .

1282 **Figure 14.** Comparison of the final modeled and measured temperature profiles at the
1283 completion of the 70-minute Palouisse B Wet heating experiment. Because the data shown
1284 in the measured profile (black) are not precisely coincident in time, the full model results
1285 (solid red and blue lines) were sub-sampled in synchrony in time (and coincide in space)
1286 with the observations. These time-synchronized model profiles are shown as dashed red and
1287 blue lines.

1288 **Figure 15.** Comparison of the final modeled and measured moisture profiles at the comple-
1289 tion of the 70-minute Palouisse B Wet heating experiment. Because the data shown in the
1290 measured profile (black) are not precisely coincident in time, the full model results (solid red
1291 and blue lines) were sub-sampled in synchrony in time (and coincide in space) with the ob-
1292 servations. These time-synchronized model profiles are shown as dashed red and blue lines.
1293 The observed data (black) suggest that the total water lost during the 70-minute experiment
1294 was 28.8% of the initial amount. The (red) model simulation indicated a 14.7% loss and the
1295 corresponding (red) synchronized-model yielded a 15.8% loss. The (blue) model simulation
1296 indicated a 27.8% loss and the corresponding (blue) synchronized-model yielded a 29.4%
1297 loss. Note there is very little recondensing soil moisture ahead of the drying front (at about
1298 35 mm depth), in agreement with Figures 11 and 12.